MBMG
Metabarcoding & Metagenomics

Metabarcoding and Metagenomics 8: 411–453 (2024)
DOI: 10.3897/mbmg.8.135082

Research Article

Comparison of the biodiversity of epiphytic diatoms in the Euphrates-Tigris rivers using morphological and metabarcoding analyses

Heba Mohamad[1], Katherina Schimani[1], Maitham Al-Shaheen[2], Nélida Abarca[1], Regine Jahn[1], Adil Al-Handal[3], Wolf-Henning Kusber[1], Jonas Zimmermann[1]

1 *Botanischer Garten und Botanisches Museum Berlin, Freie Universität Berlin, Königin-Luise-Straße 6-8, 14195 Berlin, Germany*
2 *Department of Ecology, College of Science, University of Basrah, Basrah, Iraq*
3 *Department of Biological and Environmental Sciences, University of Gothenburg, Gothenburg, Sweden*

Corresponding author: Heba Mohamad (h.mohamad@bo.berlin)

Abstract

The Euphrates-Tigris catchment area is one of the major drainage basins in the Middle East but climate change, overuse of waters and subsequent salinization has brought this region to the brink of ecological devastation. The aim of this study was to investigate the biodiversity of epiphytic diatoms in Iraq, for the first time using a combination of morphological and metabarcoding methods. 47 samples were collected at six sampling sites along the Rivers Tigris and Euphrates in northern Basra, Southern Iraq, during the summer of 2019 (dry season) and winter of 2020 (rainy season). The composition of the epiphytic diatoms in each sample was compared with both methods. The microscopic-morphological analysis of the environmental samples resulted in the identification of 284 infrageneric taxa in 59 genera. For the metabarcoding analysis the V4 region of the 18S marker gene was used and resulted in 1454 ASVs (Amplicon sequence variants) comprising 54 genera and 108 species with several ASVs belonging to the same taxa. The non-metric multidimensional scaling (NMDS) plots for morphology showed a clear seasonal effect in the diatom community composition, while the NMDS plots for 18SV4 analyses did not show a seasonal effect in community composition for the same samples. The incomplete taxonomic reference database for the studied sites turned out to be the major limitation of the molecular approach. Nevertheless, the combination of morphological and molecular methods increased the detection and identification of the diatom assemblages and laid the foundation for understanding their biodiversity in this region.

Key words: 18SV4, DNA metabarcoding, epiphytic diatoms, Euphrates-Tigris River, microscopical analysis

OPEN ACCESS

Academic editor: Hugo de Boer
Received: 19 August 2024
Accepted: 10 November 2024
Published: 13 December 2024

Citation: Mohamad H, Schimani K, Al-Shaheen M, Abarca N, Jahn R, Al-Handal A, Kusber W-H, Zimmermann J (2024) Comparison of the biodiversity of epiphytic diatoms in the Euphrates-Tigris rivers using morphological and metabarcoding analyses. Metabarcoding and Metagenomics 8: e135082. https://doi.org/10.3897/mbmg.8.135082

Copyright: © Heba Mohamad et al.
This is an open access article distributed under terms of the Creative Commons Attribution License (Attribution 4.0 International – CC BY 4.0).

Introduction

The Euphrates-Tigris area is one of the major drainage basins in the Middle East (Hassan et al. 2010). Overexploitation has pushed the water system to its ecological limits. Iraqi waterbodies suffer from salinization (Al-Handal et al. 2014) due to water losses caused by factors such as water policies during the Iraq wars, the construction of dams upstream and the impact of climate change on

the region. The country experiences minimal rainfall, particularly in the central and southern regions, leading to arid conditions (Hashim et al. 2022).

Diatoms (Bacillariophyta) are a diverse group of microalgae that play a significant role in aquatic ecosystems, serving as primary producers and contributing to the understanding of these ecosystems' functioning (Rimet et al. 2018). Several local and regional monitoring programs and networks use diatom-based indices to monitor biotic integrity and water quality (Tapolczai et al. 2024). They are globally the most commonly used bioindicators for water quality (Round et al. 1990; Visco et al. 2015), due to their unique ability to reflect ecosystem conditions (Battarbee et al. 2001; Kang et al. 2021).

Epiphytic diatoms live on the surfaces of plants, particularly submerged macrophytes. Different species of diatoms are often found on different types of macrophytes, even within the same habitat. These epiphytic communities are particularly interesting because they are attached to living plants and can interact with their hosts in various ways, potentially affecting their own community structure (Al-Handal et al. 2014). Handling of diatoms in terms of sampling, processing and storage can be managed with minor effort. Due to their silicified cell walls diatoms have the ability to survive in sediments of various composition for a long time. This quality predestines them to be universally used to examine water quality including continual changes in lakes. (Liu et al. 2017; Kang et al. 2021).

Accurate taxonomic identification of diatoms is essential for the sound evaluation of their diversity. However, diatom identification based on counting and identifying their valves using mostly light microscopy requires highly specialized taxonomic skills (Bíró et al. 2022; Stuart et al. 2024) and may lead to discrepancies in the findings depending on the researcher (Kang et al. 2021). In addition, one of the important factors that can hinder the accurate identification of classical species in diatoms is the presence of cryptic diversity. (Hadi et al. 2016; Nistal-García et al. 2021). Among the studies that have focused on the hidden diversity in diatoms are Trobajo et al. (2010); Rovira et al. (2015); Rivera et al. (2018); Pinseel et al. (2019). Furthermore, in regions where literature on the local diatom flora is not available, researchers often rely on European floras, which may force identifications into the existing taxonomic concepts, potentially overlooking local variation or unique species.

To optimize diatom identification, DNA metabarcoding is increasingly used because it is generally less time-consuming and may be more accurate than morphological identification. This method enables the concurrent identification of numerous species from environmental samples (Ruppert et al. 2019; Kang et al. 2021).

This method has been used to investigate freshwater diatom biodiversity (Mora et al. 2019) and has also been leveraged for the evaluation of water quality with a focus on benthic diatoms (Vasselon et al. 2017; Bailet et al. 2019; Mortágua et al. 2019; Kelly et al. 2020; Pérez-Burillo et al. 2020). It has also been applied to some extent to marine environments (Malviya et al. 2016; Piredda et al. 2018; Schimani et al. 2023). Even though the DNA barcoding reference database needs to grow and expand, metabarcoding has proven to be an efficient tool for surveying diatom communities in comparison to morphological analyses (Zimmermann et al. 2015; Keck et al. 2018; Rivera et al. 2018).

While metabarcoding has seen widespread adoption globally over the past decade for diatom analysis (Burki et al. 2021; Almandoz et al. 2024), there is a notable absence of such studies in Iraq. Given that our current understanding of diatoms largely relies on microscopic-morphological studies, it seemed opportune

to combine both approaches to enrich our comprehension of the epiphytic diatom community composition in this area. By integrating metabarcoding and traditional microscopic analysis, a more comprehensive and detailed insight into the diversity and dynamics of diatom populations within the region can be obtained.

In this study, the aim was to identify the biodiversity of epiphytic diatoms using metabarcoding of diatom 18SV4 DNA and classical methods (light and scanning electron microscopy), followed by a comparison of differences in diatom species and abundance inventories obtained by both methods. This analysis was conducted on a set of 47 samples collected from two different water bodies in Iraq, namely the River Tigris and River Euphrates.

Materials and methods

Study area and sample collection

Epiphytic diatoms were sampled from freshwaters during the summer of 2019 and winter of 2020, encompassing 47 samples from six sites across two water bodies in Iraq: River Tigris in the city of Al-Qurnah, and River Euphrates in the city of Al-Midaina (Fig. 1). Due to the absence of stones as habitats at either of the sampling stations, samples were collected separately from 11 different taxa of macrophytes, including *Phragmites australis*, *Typha domingensis*, *Ceratophyllum demersum*, *Myriophyllum spicatum*, *Potamogeton crispus*, *Potamogeton perfoliatus*, *Potamogeton* sp., *Cladophora glomerata*, *Cladophora* spp., *Najas minor* and *Aster tripolium* (Table 1). At least five stems and branches in good condition of a macrophyte or macroalga were put into a plastic bag, and then shaken vigorously with distilled water to dislodge attached diatoms. The resulting suspension was poured into a plastic container and preserved with 70% alcohol for transportation to the laboratory at the Botanic Garden and Botanical Museum (BGBM), Freie Universität Berlin. Each sample was divided into two portions for subsequent analysis, including 1) the morphological identification of the diatom community, and 2) a community analysis conducted via DNA metabarcoding.

Physical and chemical parameters

Water samples for physical-chemical parameters analyses were taken at the same sites where diatom sampling was carried out (Table 2). These included air and water temperature (°C), pH, conductivity ($\mu S.cm^{-1}$), dissolved oxygen ($mg.l^{-1}$), water transparency (cm), turbidity (NTU), and total alkalinity ($mg.l^{-1}$), using different instruments. Nitrate ($mg.l^{-1}$), phosphate ($mg.l^{-1}$) and silicate ($mg.l^{-1}$) were measured according to Strickland and Parsons (1972), Lind (1979) and APHA (1999, 2005).

Microscopical analysis

Environmental samples underwent treatment with 35% hydrogen peroxide at room temperature to facilitate the oxidation of organic materials. Following this, the samples were thoroughly washed with distilled water, employing the method outlined by Mora et al. (2019). The cleaned frustules and valves were air-dried on coverslips and mounted on microscopic slides using the high refractive index medium Naphrax®.

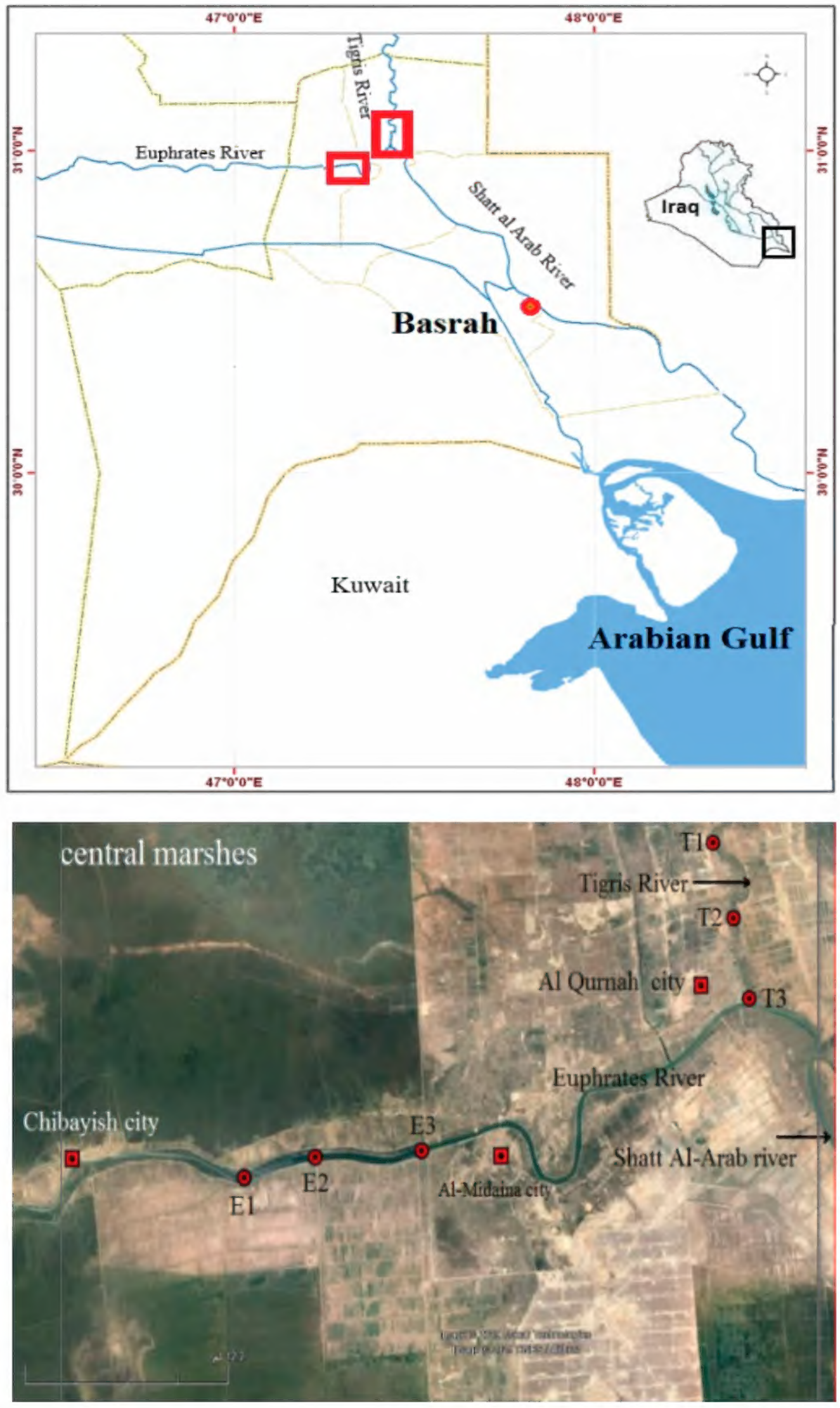

Figure 1. Area of study: Location of the six sampling sites in the Rivers Tigris and Euphrates indicated by red dots. The numbers next to the red dots refer to the name of the sampling site in Table 1.

To investigate the composition of epiphytic diatoms, each environmental sample was examined using light microscopy (LM). The Zeiss Axioplan microscope equipped with differential interference contrast (DIC) was employed, using a Zeiss 100× Plan Apochromat objective with the AXIOCAM MRc camera. All samples were measured using the AxioVision software.

Table 1. Sampling sites with information on the sampling station, voucher, georeference, substrates, taxon richness and Shannon diversity index. The samples were collected by Maitham Al-Shaheen. Legend: T = Tigris River, E = Euphrates River, S = summer, W = winter, LM = microscopic morphology, M = metabarcoding. Substrates: *Ph. australis* (Cav.) Steud., *T. domingensis* Pers., *C. demersum* L., *M. spicatum* L., *P. crispus* L., *P. perfoliatus* L., *Potamogeton* sp., *C. glomerata* (L.) Kütz, *Cladophora* spp., *N. minor* All. and *A. tripolium* L.

Sample	Voucher at B	Latitude, Longitude	Substrates	light microscopic		Metabarcoding	
				Taxon richness	Shannon index	Taxon richness	Shannon index
S.T1.1	B 50 0021402	31.08990, -47.42780	*Ph. australis*	35	3.17	105	3.38
S.T2.2	B 50 0021403	31.05479, -47.43479	*Ph. australis*	35	3.07	103	3.48
S.T2.3	B 50 0021404	31.05479, -47.43479	*C. demersum*	34	3.08	57	2.37
S.T3.4	B 50 0021405	31.00689, -47.44049	*Ph. australis*	23	2.48	141	3.38
S.T3.5	B 50 0021406	31.00689, -47.44049	*C. demersum*	35	3.20	49	2.22
S.E1.6	B 50 0021407	30.94654, -47.09925	*Ph. australis*	25	2.70	245	3.96
S.E1.7	B 50 0021408	30.94654, -47.09925	*T. domingensis*	35	3.22	24	2.62
S.E1.8	B 50 0021409	30.94654, -47.09925	*C. demersum*	33	3.19	187	3.85
S.E1.9	B 50 0021410	30.94654, -47.09925	*M. spicatum*	21	2.56	189	4.25
S.E1.10	B 50 0021411	30.94654, -47.09925	*P. perfoliatus*	36	3.19	–	–
S.E1.11	B 50 0021412	30.94654, -47.09925	*N. minor*	43	3.42	26	2.75
S.E2.12	B 50 0021413	30.95243, -47.14902	*Ph. australis*	30	3.00	103	3.64
S.E2.13	B 50 0021414	30.95243, -47.14902	*T. domingensis*	31	3.15	52	2.84
S.E2.14	B 50 0021415	30.95243, -47.14902	*C. demersum*	33	3.13	94	3.81
S.E2.15	B 50 0021416	30.95243, -47.14902	*P. perfoliatus*	30	2.92	158	4.00
S.E2.16	B 50 0021417	30.95243, -47.14902	*N. minor*	30	3.26	275	2.78
S.E3.17	B 50 0021418	30.94976, -47.21792	*Ph. australis*	21	2.80	53	0.43
S.E3.18	B 50 0021419	30.94976, -47.21792	*C. demersum*	25	2.93	158	3.09
S.E3.19	B 50 0021420	30.94976, -47.21792	*P. perfoliatus*	24	2.81	14	3.58
S.E3.20	B 50 0021421	30.94976, -47.21792	*N. minor*	31	3.16	172	2.56
W.T1.21	B 50 0021422	31.08990, -47.42780	*Ph. australis*	31	3.15	134	4.06
W.T1.22	B 50 0021423	31.08990, -47.42780	*C. demersum*	30	2.96	116	3.43
W.T2.23	B 50 0021424	31.05479, -47.43479	*Ph. australis*	37	3.30	93	3.65
W.T2.24	B 50 0021425	31.05479, -47.43479	*T. domingensis*	26	2.86	–	–
W.T2.25	B 50 0021426	31.05479, -47.43479	*Potamogeton sp.*	14	1.84	198	1.60
W.T3.26	B 50 0021427	31.00689, -47.44049	*Ph. australis*	36	3.18	129	1.50
W.T3.27	B 50 0021428	31.00689, -47.44049	*C. demersum*	21	2.58	32	1.56
W.T3.28	B 50 0021429	31.00689, -47.44049	*P. crispus*	14	2.34	102	3.31
W.T3.29	B 50 0021430	31.00689, -47.44049	*C. glomerata*	22	2.30	140	3.13
W.E1.30	B 50 0021431	30.94654, -47.09925	*Ph. australis*	26	2.77	143	2.58
W.E1.31	B 50 0021432	30.94654, -47.09925	*T. domingensis*	23	2.40	157	2.21
W.E1.32	B 50 0021435	30.94654, -47.09925	*N. minor*	18	2.38	136	2.43
W.E1.33	B 50 0021433	30.94654, -47.09925	*C. demersum*	32	3.03	129	2.99
W.E1.34	B 50 0021434	30.94654, -47.09925	*P. crispus*	12	2.10	345	3.13
W.E2.35	B 50 0021436	30.95243, -47.14902	*Ph. australis*	22	2.57	263	3.89
W.E2.36	B 50 0021438	30.95243, -47.14902	*T. domingensis*	12	2.30	–	–
W.E2.37	B 50 0021442	30.95243, -47.14902	*A. tripolium*	19	2.55	18	1.49
W.E2.38	B 50 0021437	30.95243, -47.14902	*C. demersum*	31	3.14	249	2.73
W.E2.39	B 50 0021441	30.95243, -47.14902	*P. perfoliatus*	16	2.38	129	2.24
W.E2.40	B 50 0021440	30.95243, -47.14902	*Cladophora* spp.	15	2.02	–	–
W.E2.41	B 50 0021439	30.95243, -47.14902	*P. crispus*	17	2.34	223	2.30
W.E3.42	B 50 0021445	30.94976, -47.21792	*P. crispus*	15	2.37	45	3.09
W.E3.43	B 50 0021444	30.94976, -47.21792	*C. demersum*	27	2.79	5	1.47
W.E3.44	B 50 0021443	30.94976, -47.21792	*Ph. australis*	31	3.13	139	3.82
W.E3.45	B 50 0021447	30.94976, -47.21792	*N. minor*	21	2.71	82	1.30
W.E3.46	B 50 0021446	30.94976, -47.21792	*P. crispus*	21	2.38	191	4.38
W.E3.47	B 50 0021448	30.94976, -47.21792	*N. minor*	11	1.27	145	3.51

Table 2. Physical and chemical composition of the water at the sampling stations in August 2019 (summer) and February 2020 (winter). AT = Air Temperature in °C; WT = Water temperature in °C; PH = Hydrogen Ion Concentration; Cond = Specific Conductivity Corrected at 25 °C (µS.cm^{-1}); DO = Dissolved Oxygen (mg/L); Turb = Turbidity (NTU); TA = Total Alkalinity mg.l^{-1}; Trans = Transparency (cm); $NO3^{-}$ = Nitrate Nitrogen (mg.l^{-1}); $PO4^{-3}$ = Phosphat Phosphate (mg.l^{-1}) and SiO3 = Reactive Silicate (mg.l^{-1}).

River	Tigris River						Euphrates River					
Site	T1		T2		T3		E1		E2		E3	
Parameters	S	W	S	W	S	W	S	W	S	W	S	W
AT (°C)	39	21.7	35	22.5	34.5	20.1	38	24.8	41.5	25.1	44	25.4
WT (°C)	32.1	17.4	30.6	18.1	30.2	16.6	35.5	20.5	36.7	20.6	36.5	21.2
pH	8.18	8.45	8.19	8.2	8.19	8.15	7.67	8.16	8.21	8.32	8.13	8.12
Cond (µS.cm^{-1})	1225	2160	1135	2140	1160	2190	3198	4470	3065	4475	3735	4860
DO (mg.l^{-1})	6.8	10.1	7	9.2	7.2	10.6	8.3	7.6	6.1	8.4	6.7	9.4
Turb (NTU)	55	47.4	59	45	66	49.5	4.96	13.1	7.85	7.98	12.5	8.9
Trans (cm)	22	35	25	30	25	24	85	200	76	191	72	183
TA (mg.l^{-1})	70	139	73	144	75	150	58	145	46	138	36	130
NO_3^{-}(mg.l^{-1})	1.8	2.4	1.5	1.2	1.56	1.9	0.8	1.1	0.7	1.1	1.15	1.2
PO_4^{-3} (mg.l^{-1})	0.104	1.02	0.1755	0.31	0.182	0.33	0.195	0.3	0.130	0.38	0.065	0.24
SiO3 (mg.l^{-1})	6	3.5	8	4.3	8	5.7	16	9	9	9.2	17	10.6

To document the presence and abundance of each diatom taxon across all sampling sites, a minimum of 400 valves were counted in each sample, and subsequently, the relative abundance of each taxon was calculated. When more details were needed, aliquots of cleaned sample material for scanning electron microscopy observations were mounted on stubs and observed under a Hitachi FE 8010 scanning electron microscope (SEM) operated at 1.0 kV. Samples, slides and pictures are deposited in a database at the Diatom Collection of the Botanic Garden and Botanical Museum Berlin, Freie Universität Berlin.

Morphological analysis

The morphological information by both LM and scanning electron microscopy (SEM) was used to identify the diatoms to the lowest taxonomical rank possible (Table 3). Whenever possible, identification literature from the region was consulted, but often European literature was used due to the lack of specific identification literature for the region. Morphological identification followed predominantly Al-Handal and Al-Shaheen (2019), Lange-Bertalot et al. (2017), Krammer (2002), Krammer and Lange-Bertalot (1986, 1991), Witkowski et al. (2000), and Reichardt (2018). For nomenclatural authors and references for identification of each name, see Table 3. Species marked as new to Iraq are species not included in Maulood et al. (2013) and Al-Handal and Al-Shaheen (2019) as well as missing in the Distribution section in AlgaeBase (Guiry and Guiry 2024).

Metabarcoding analyses

DNA extraction and PCR amplification

Samples were centrifuged at 11. 000 rpm for 5 minutes. The supernatant was discarded and the DNA extracted from the pellet following the standard protocol proposed with the NucleoSpin ® Soil Kit of Macherey and Nagel (MN-Soil). DNA samples were stored at -20 °C for future use and finally deposited in the Berlin collection of the DNA bank network (Gemeinholzer et al. 2011).

The V4 region of the 18S rRNA gene for 47 samples was amplified by PCR using primers DIV4 for: 5'-GCGGTAATTCCAGCTCCAATAG-3' and DIV4rev3: 5' - CTCTGACAATGGAATACGAATA-3', following the protocols and primers outlined by Visco et al. (2015), with modifications for 300-bp paired-end sequencing on the Illumina MiSeq, as adapted from Zimmermann et al. (2011). PCR amplifications were performed in duplicate per sample, using two different polymerases, each in a total volume of 25 µL, to increase amplification success across all samples. This approach was necessary as some samples did not amplify successfully with the first polymerase but yielded successful results with the second. The PCR mix with the first polymerase contained 0.5 µL dNTP mix (25 mM each dNTP), 0.25 µL BSA (10 mg/mL), 0.25 µL DMSO, 1 µL of each forward and reverse primers (10 pm/µL), 0.4 µL of Herculase II Fusion DNA Polymerase (Agilent Technologies Inc., Santa Clara, California, USA), 5 µL Herculase II reaction buffer, 1 µL of template DNA (20 ng/µL) and 15.6 µL of HPLC grade water. The PCR regime included an initial denaturation at 94 °C (2 minutes) followed by 35 cycles consisting of denaturation at 94 °C (45 seconds), annealing at 52 °C (45 seconds), elongation at 72 °C (1 minute) and a final elongation at 72 °C (10 minutes).

The PCR mix with the second polymerase contained each in a total volume of 25 µL: 2 µL dNTP (Takara), 1.25 µL BSA (10 mg/mL), 1.25 µL of each forward and reverse primers (10 pm/µL), 0.15 µL of Takara DNA Polymerase, 2.5 µL buffer (10×), 1 µL of template DNA (20 ng/µL) and 16.1 µL of HPLC grade water. The PCR regime included an initial denaturation at 95 °C (2 minutes) followed by 33 cycles consisting of denaturation at 95 °C (1 minute), annealing at 54 °C (1 minute), elongation at 72 °C (1 minute) and a final elongation at 72 °C (5 minutes).

Size and quantification of DNA fragments was measured with the Fragment Analyzer™ (dsDNA 930 Reagent Kit, 75 bp-20000 bp) system was followed for quality control of PCR products. The DNA fragment was considered valid when the size was between 390 and 450 bps and the concentration was greater than 1 ng/µL

Aliquot of 25 µL of the amplicons were purified using HighPrep PCR paramagnetic beads (Magbio Genomics). A second PCR run, the indexing PCR, was conducted on the purified samples to ligate a unique combination of tags to the 5´ end of the primer. Indexing PCR reactions of 25 µL were conducted as follows: 0.25 dNTP mix, 1 µL DMSO, 0.625 µL of each primer, 0.25 µL of Herculase, 5 µL Herculase II reaction buffer, 10 µL of template DNA and 7.25 µL of HPLC grade water. The indexing PCR regime started with denaturation at 95 °C (2 minutes), then 8 cycles consisting of denaturation at 95 °C (20 seconds), annealing at 52 °C (30 seconds), elongation at 72 °C (30 seconds) and a final elongation at 72 °C (3 minutes). PCR fragments' size concentrations were checked by Fragment Analyzer (1× TE Dilution Buffer). Products were purified using HighPrep PCR paramagnetic beads and quantified using Quant (2.0)-iT PicoGreen dsDNA Assay Kit (Invitrogen, Carlsbad, California, USA) and adjusted to a concentration of 20 ng/µL. Library preparation was performed using MiSeq Reagent Kit V3 (300 bp paired-end reads) (Illumina, San Diego, California, USA). MiSeq sequencing with 600 cycles was conducted at the Berlin Center for Genomics in Biodiversity Research (BeGenDiv) of the Berlin Brandenburg Institute of Advanced Biodiversity Research (BBiB). Raw demultiplexed reads were deposited at GenBanks Sequence Read Archive and are available under project number PRJNA1148423.

Table 3. List of all species observed in light microscopy (LM) with author(s) and reference(s) for identification. (r) behind the taxon name indicates that it was a rare species just observed in a thorough scan of the slide. Species new to the flora of Iraq are marked by an asterisk. cf. (confer) before the epithet indicates taxonomic uncertainty, aff. (affinis): indicates that the specimen is thought to be closely similar to the specified species but is not confirmed as that species. and 'sp.' (species) was used when the taxon showed no similarity to any known species after thorough literature review, L = valve length [µm], W = valve width [µm], S = stria number in 10 µm, F = fibulae in 10 µm, D = diameter. TS = Tigris summer, TW = Tigris winter, ES = Euphrates summer, EW = Euphrates winter.

Taxa, Author		Reference	L	W	S	F	D	TS	TW	ES	EW
CENTRIC											
Aulacoseira granulata (Ehrenberg) Simonsen	(r)	Krammer & Lange-Bertalot 1991 (2/3): p. 22, pl. 18, figs 1–12; Al-Handal and Al-Shaheen 2019: p. 11, Pl. 11, fig. 1					9–11		x		
Aulacoseira ambigua (Grunow) Simonsen	Fig. 2M	Krammer & Lange-Bertalot 1991 (2/3): p. 25, pl. 21, figs 1–16					8–12		x		
Cyclotella atomus Hustedt	(r)	Al-Handal & Al-Shaheen 2019: p. 12, Pl. 1, figs 5–6; Krammer & Lange-Bertalot 1991 (2/3): p. 53, pl. 51, figs 19–21					5.3–6.5		x		
Cyclotella meneghiniana Kützing	Fig. 2L	Al-Handal & Al-Shaheen: p. 13, Pl. 1, figs 8–10; Krammer & Lange-Bertalot 1991 (2/3): p. 44, pl. 44, figs 1–10					7–33.5	x	x	x	x
Cyclotella ocellata Pantocsek	(r)	Krammer & Lange-Bertalot 1991 (2/3): p.51, pl. 51, figs 1–5					6–19.7			x	x
Cyclotella cf. *ocellata* Pantocsek	(r)	Krammer & Lange-Bertalot 1991 (2/3): p.51, pl. 51, figs 1–5					17		x		
Cyclotella radiosa (Grunow) Lemmermann	(r)	Al-Handal & Al-Shaheen 2019: p. 14, Pl. 1, fig. 12					16–17			x	
Cyclotella tripartita Håkanasson	(r), (*)	Krammer & Lange-Bertalot 1991 (2/3): p.49, pl. 48, figs 4–7					15–15.8		x	x	
Cyclotella sp. 1	Fig. 2J, K						4–4.7			x	x
Cyclotella sp. 2	(r)						7–8	x			
Melosira varians C.Agardh	(r)	Lange-Bertalot et al. 2017: p. 368, pl. 1, Figs 6–10; Krammer and Lange-Bertalot 1991 (2/3): p. 7, pl. 4, figs 1–8					15–20		x		
Stephanodiscus alpinus Hustedt	Fig. 2E, F	Krammer and Lange-Bertalot 1991 (2/3): p.70, pl. 72, figs 3a-4					18.8–21.7		x		x
Stephanodiscus hantzschii Grunow	Fig. 2D	Krammer and Lange-Bertalot 1991 (2/3): p.73, pl. 75, figs 4–14; pl. 76, Figs 1–3					10–13		x		
Stephanodiscus hantzschii var. *tenuis* (Hustedt) Håkansson & Stoermer	(*), Fig. 2C	Krammer and Lange-Bertalot 1991 (2/3): p.74, pl. 75, figs 12–14;					13–13.7		x		
Stephanodiscus neoastraea Håkansson & Hickel	Fig. 2A, B	Krammer & Lange-Bertalot 1991 (2/3): p.68, pl. 69, Fig. 3, pl. 71, Figs 3a-5b					16.4–32.6		x		
Cyclostephanos invisitatus (M.H. Hohn & Hellerman) E.C. Theriot, Stoermer & Håkanasson	(*) Fig. 2H, I	Krammer & Lange-Bertalot 1991 (2/3): p. 63, pl. 67, figs 3–4					9–9.7	x	x		
Thalassiosira lacustris (Grunow) G.R.Hasle ≡ *Lineaperpetua lacustris* (Grunow) P.Yu, Q.-M.You, Kociolek & Wang	Fig. 2G	Smucker et al. 2008: p. 205, figs 2–7, Al-Handal & Al-Shaheen 2019: p. 12, pl. 1, figs 2–3 (as *Thalassiosira bramaputrae*)					19.7–32	x	x		
ARAPHID											
Ctenophora pulchella (Ralfs ex Kützing) D.M. Williams & Round	(r)	Al-Handal & Al-Shaheen 2019: p. 20, pl. 5, figs 3,4	69–70	5.5–6	13–14					x	
Ctenophora sp.1	(r)		82–89	6–7	14–15			x			

Taxa, Author		Reference	L	W	S	F	D	TS	TW	ES	EW
Diatoma moniliformis (Kützing) D.M.Williams	Fig. 2AA, AB	Lange-Bertalot et al. 2017: p. 185, pl. 3, figs 5–6	6.4–27.3	4–5	7–8						x
Diatoma cf. *moniliformis* (Kützing) D.M.Williams	(r)	Lange-Bertalot et al. 2017: p. 185, pl. 3, figs 5–6	42.5–45	4.5–5	8–9						x
Diatoma vulgaris Bory	Fig. 2Y, Z	Lange-Bertalot et al. 2017: p. 187, pl. 4, figs 5–6; Al-Handal & Al-Shaheen 2019: p. 21, pl. 5, fig. 7	21–42.5	12.5–14.5	5–7				x		
Fragilaria crotonensis Kitton	(r)	Krammer & Lange-Bertalot 1991 (2/3): p. 130, pl. 116, figs 1–4	76–86.7	3.5–4	14–16				x		
Fragilaria koensabbei Al-Handal & Al-Shaheen	Fig. 3G	Al-Handal & Al-Shaheen 2019: p. 22, pl. 6, figs 1–9	160–213	5–6.5	13–15			x	x	x	x
Tabularia fasciculata (C.Agardh) D.M.Williams & Round	Fig. 2AD	Lange-Bertalot et al. 2017: p. 591, pl. 5, figs 1–2						x	x	x	x
Ulnaria acus (Kützing) Aboal	Fig. 3C	Al-Handal & Al-Shaheen 2019: p. 26, pl. 7, fig. 1	117–190	4–5	12–15					x	
Ulnaria capitata (Ehrenberg) Compère	Fig. 3A	Al-Handal & Al-Shaheen 2019: p. 26, pl. 7, figs 4–5; Krammer & Lange-Bertalot 1991: p. 143, pl. 122, figs 1–8	264–288	7–8	10–11				x	x	x
Ulnaria danica (Kützing) Compère & Bukhtiyarova	Fig. 3B	Al-Handal & Al-Shaheen 2019: p. 27, pl. 7, figs 6–7	212–311	4.2–5.8	9–11				x		x
Ulnaria delicatissima var. *angustissima* (Grunow) Aboal & P.C.Silva	Fig. 3D	Al-Handal & Al-Shaheen 2019: p. 27, pl. 7, fig. 8	140–171	3.4–4	12–13				x	x	x
Ulnaria cf. *obtusa* (W.Smith) E.Reichardt	(r)	Reichardt 2018: p. 100, pl. 23	180–200	7–8	9–10				x		
Ulnaria ulna (Nitzsch) Compère	Fig. 3F	Al-Handal & Al-Shaheen 2019: p. 27, pl. 7, figs 9–10	200–230	6–8	9–11			x	x	x	x
Ulnaria ulna var. *claviceps* (Hustedt) Compère	Fig. 3E	Al-Handal & Al-Shaheen 2019: p. 27, pl. 7, figs 11–13	195–200	6–7	8–10					x	
Ulnaria sp.1	(r)									x	x
Ulnaria sp.2	(r)									x	
Ulnaria sp.3	(r)									x	
Synedropsis abuflosensis Al-Handal, Al-Shaheen & Al-Saedy	Fig. 2AC	Al-Handal et al. 2022: p. 43, figs A-G	31–38 (42)	2.5–2.8						x	
MONORAPHID											
Achnanthes brevipes var. *brevipes* C.Agardh	(r), (*)	Lange-Bertalot et al. 2017: p. 78, pl. 22, figs 1–5; Witkowski et al. 2000: p. 86, pl. 45, figs 3–10	42.7–47	11–11.2	10–11					x	x
Achnanthidium minutissimum complex (Kützing) Czarnecki	Fig. 2S, T	Lange-Bertalot et al. 2017: p. 87, pl. 24, figs 15–21; Al-Handal & Al-Shaheen 2019: p. 47, pl. 16, figs 1–4	10–21	3–4				x	x	x	x
Achnanthidium gracillimum (F.Meister) Lange-Bertalot	(r), (*)	Lange-Bertalot et al. 2017: p. 85, pl. 24, figs 72–77	13–20	3.5–3.7					x		
Achnanthidium neomicrocephalum Lange-Bertalot & Staab	(r), (*)	Reichardt 2018: p. 106, pl. 62, figs 91–106	28.5–30	2.8–3						x	x
Cocconeis pediculus Ehrenberg	(r)	Al-Handal & Al-Shaheen 2019: p. 47, pl. 15, figs 10–11; Lange-Bertalot et al. 2017: p. 139, pl. 20, figs 17–19	29–30	23–24	18–19				x		
Cocconeis euglypta Ehrenberg	Fig. 2Q, R	Al-Handal & Al-Shaheen 2019: p. 46, pl. 15, figs 3–9	12–30	8–17				x	x	x	x
Cocconeis placentula Ehrenberg complex	Fig. 2N-P	Al-Handal & Al-Shaheen 2019: p. 47, pl. 15, figs 3–5; Lange-Bertalot et al. 2017: p. 139, pl. 20, Figs 1–2	12–48	8–25	22–25			x	x	x	x
Lemnicola hungarica (Grunow) Round & Basson	Fig. 2U-X	Lange-Bertalot et al. 2017: p. 354, pl. 26, figs 71–77	21–45	7–8.5	20–21			x		x	
ASYMMETRICAL BIRAPHID											
Amphora copulata (KÜTZING) Schoeman & R.E.M.Archibald	Fig. 4K	Lange-Bertalot et al. 2017: p. 98, pl. 93, figs 4–8, Levkov 2009 (V5): p. 49, pl. 46, figs 13–23	23–35.5	6–7	14–15			x	x	x	x
Amphora sp. 1	(r)		54–54.5	10–11	10–10.5						x

Taxa, Author		Reference	L	W	S	F	D	TS	TW	ES	EW
Cymbella cymbiformis C.Agardh	Fig. 4A	Lange-Bertalot et al. 2017: p.159, pl. 82, figs 1–11; Al-Handal & Al-Shaheen 2019: p. 35, pl. 10, fig. 8	40–96	13–16	8–10				x	x	x
Cymbella cf. *cymbiformis* C.Agardh	Fig. 4D	Lange-Bertalot et al. 2017: p.159, pl. 82, figs 1–11; Al-Handal & Al-Shaheen 2019: p. 35, pl. 10, fig. 8	30–36	12–12.5	20–22						x
Cymbella neocistula Krammer	Fig. 4C	Lange-Bertalot et al. 2017: p.164, pl. 81, figs 1–5	43.5–54(85)	13–15	9–11				x		x
Cymbella stigmaphora Østrup	(*), Fig. 4G	Krammer 2002 (V3): p.135, pl. 154, figs 18–23	38.5–43	9–11	10–11						x
Cymbella tumida (Brébisson) Van Heurck	Fig. 4B	Lange-Bertalot et al. 2017: p. 168, pl. 83, figs 5–6	36–85	16–21	9–11			x	x	x	x
Cymbella cf. *tumida* (Brébisson) Van Heurck	(r)	Lange-Bertalot et al. 2017: p. 168, pl. 83, figs 5–6	33	14.5	12				x		
Cymbella sumatrensis Hustedt	Fig. 4E	Krammer 2002 (V3): p. 72, pl. 54, figs 2–17	30–33	9–9.5	11.12				x	x	x
Cymbella hustedtii Krasske	Fig. 4F	Krammer 2002 (V3): p. 137, pl. 160, figs 7–13	15–22	6.5–8	12–14				x	x	x
Cymbella sp. 1	(r)		94–95	14–14.5	9–10						x
Cymbella sp. 2	(r)		31–48	8.7–11	9–11						x
Cymbella sp. 3	(r)		40–42	13–14	6–6.5					x	
Cymbella sp. 4	(r)		23–35	8–8.5	10–11						x
Encyonema vulgare var. *vulgare* Krammer	(*), Fig. 4O	Lange-Bertalot et al. 2017: p. 210, pl. 89, figs 30–32	29–60	9–14	7.5–10			x	x	x	x
Encyonema sp. 1	Fig. 4P		65–70	13–15	8–9					x	
Encyonopsis cf. *microcephala* (Grunow) Krammer	Fig. 4V	Lange-Bertalot et al. 2017: p. 213, pl. 91, figs 35–39	13–16.5	3.5–4	22–24				x	x	x
Encyonopsis cf. *minuta* Krammer & E.Reichardt	(*), Fig. 4U	Lange-Bertalot et al. 2017: p. 214, pl. 91, figs 25–34	10–14	3.2–3.5	20–22						x
Gomphonella coxiae R.Jahn & N.Abarca	(*), Fig. 5AA, AB	Jahn et al. 2019: p. 236, pl.13, figs A–O	42–52.7	7.88.7	10–12						x
Gomphonella olivacea (Hornemann) Rabenhorst	Fig. 5Y, Z	Jahn et al. 2019: p. 236, pl. 7, figs C–E	16–35.5	7–8.6	9–12				x		x
Gomphonema olivaceolacuum (Lange-Bertalot & E.Reichardt) Lange-Bertalot et Reichardt	(r), (*)	Lange-Bertalot et al. 2017: p. 313, pl. 97, figs 17–19	35–38	8–9	12–13				x		
Gomphonema affine Kützing	Fig. 5A	Krammer & Lange-Bertalot 1986 (2/1): p. 366, pl. 161, figs 1–3; Levkov et al. 2016 (V8): p. 24, pl. 41, figs 1–12	64–65	11–11.7	8–9			x			
Gomphonema cf. *affine* Kützing	Fig. 5B, C	Krammer & Lange-Bertalot 1986 (2/1): p. 366, pl. 161, figs 1–3; Levkov et al. 2016 (V8): p. 24, pl. 41, figs 1–12	30–80	12.5–15.7	8–13			x		x	
Gomphonema auritum A.Braun ex Kützing	(*), Fig. 5N	Lange-Bertalot et al. 2017: p. 300, pl. 100, figs 16–20	22–33	5–6	12–13					x	x
Gomphonema cf. *augur* Lange-Bertalot	(r)	Krammer & Lange-Bertalot 1986 (2/1): p. 363, pl. 157, fig. 7	53–54	12–13	8–9			x			
Gomphonema parvulum (Kützing) Kützing	Fig. 5O, P	Levkov et al. 2016 (V8): p. 98, pl. 102, figs 20–28	15–25	5–7	13–14			x			x
Gomphonema graciledictum E.Reichardt	(*), Fig. 5L	Lange-Bertalot et al. 2017: p. 297, pl. 100, figs 11–15; Levkov et al. 2016 (V8): p. 53, pl. 108, figs 1–34	25–57	6–8	13–15					x	x
Gomphonema vibrio Ehrenberg	Fig. 5F	Lange-Bertalot et al. 2017: p. 324, pl. 98, figs 1–5	40–66	7–9	8–10				x		x
Gomphonema lagenula Kützing	(r)	Levkov et al. 2016 (V8): p. 71, pl. 102, figs 39–47	25–26.5	7–7.5	12–13			x			
Gomphonema cf. *lagenula* Kützing	Fig. 5Q	Levkov et al. 2016 (V8): p. 71, pl. 102, figs 39–47	18–29	6.5–8	12–14			x			
Gomphonema hebridense W.Gregory	(*), Fig. 5M	Lange-Bertalot et al. 2017: p. 306, pl. 100, figs 6–10; Levkov et al. 2016 (V8): p. 54, pl. 134, figs 1–28	28–60	5.5–7	12–15					x	

Taxa, Author		Reference	L	W	S	F	D	TS	TW	ES	EW
Gomphonema cf. *hebridense* W.Gregory	Fig. 5G	Lange-Bertalot et al. 2017: p. 306, pl. 100, figs 6–10; Levkov et al. 2016 (V8): p. 54, pl. 134, figs 1–28	20–51	5–8	12–14					x	
Gomphonema naviculoides W.Smith	(*), Fig. 5D	Levkov et al. 2016 (V8): p. 89, pl. 42, figs 1–19	42–63	8–9	11–13					x	x
Gomphonema pseudoaugur Lange-Bertalot	(*), Fig. 5H, I	Lange-Bertalot et al. 2017: p. 318, pl. 95, figs 1–4	35–51	8–8.6	10–12				x		x
Gomphonema lateripunctatum E.Reichardt & Lange-Bertalot	(r), (*)	Levkov et al. 2016 (V8): p. 73, pl. 143, figs 1–31	31–34	6–6.5	8–9					x	
Gomphonema pumilum var. *pumilum* (Grunow) E.Reichardt et Lange-Bertalot	Fig. 5R, S	Lange-Bertalot et al. 2017: p. 319, pl. 99, figs 10–14	15–20	4.2–5	11–12				x		
Gomphonema angustum C.Agardh	(r), (*)	Krammer & Lange-Bertalot 1986 (2/1): p. 370, pl. 164, figs 1–16	27–44	5.7–7	10–12						x
Gomphonema cf. *pseudaffine* Levkov, Mitic-Kopanja & E.Reichardt	Fig. 5X	Levkov et al. 2016 (V8): p. 107, pl. 71, figs 1–25	25–29	9–10	12–13			x			
Gomphonema cf. *subclavatum* (Grunow) Grunow	Fig. 5E	Lange-Bertalot et al. 2017: p. 321, pl. 97, figs 21–24	46–58.5	8–9.5	9–10						x
Gomphonema gracile Ehrenberg	(r)	Krammer & Lange-Bertalot 1986 (2/1): p. 361, pl. 156, fig. 9	36–34	8–8.5	13–15						x
Gomphonema cf. *parvuliforme* Levkov, Mitic-Kopanja & E.Reichardt	(r)	Levkov et al. 2016 (V8): p. 56, pl. 105, figs 10–12	14–14.5	5.5–6	14–15						x
Gomphonema cf. *truncatum* Ehrenberg	Fig. 5K	Levkov et al. 2016 (V8): p. 130, pl. 14, figs 1–5	33.8–55	9–12	11–12				x		
Gomphonema capitatum complex Ehrenberg	Fig. 5T-W	Reichardt 2001: p. 192, pl. 1, fig. 20	20–32.7	7–10	10–13				x	x	x
Gomphonema cf. *laticollum* E.Reichardt	Fig. 5J	Reichardt 2001: p. 199, pl. 5, figs 1–11	36–56	9–11.5	9–12				x		x
Gomphonema sp. 1	(r)		20–22	6–7	12–15						x
Gomphonema sp. 2	(r)		18–21	5–6	14–15						x
Halamphora veneta (Kützing) Levkov	Fig. 4I	Levkov 2009 (V5): p. 242, pl. 102, figs 17–30	13–35	4.9–6	20–22			x	x	x	x
Halamphora cf. *veneta* (Kützing) Levkov	(r)	Levkov 2009 (V5): p. 242, pl. 102, figs 17–30	36–45	5–6	20–21						x
Halamphora coffeaeformis (C.Agardh) Levkov	Fig. 4J	Levkov 2009 (V5): p. 179, pl. 91, figs 1–14	25–27	4.5–5.7	19–20				x		
Halamphora cf. *coffeaeformis* (C.Agardh) Levkov	Fig. 4H	Levkov 2009 (V5): p. 179, pl. 91, figs 1–14	17–51	4–6	20–22				x	x	x
Halamphora montana (Krasske) Levkov	(r), (*)	Levkov 2009 (V5): p. 207, pl. 93, figs 10–19	15–15.5	3.5–3.9				x			
Halamphora oligotraphenta (Lange-Bertalot) Levkov	(r)	Levkov 2009 (V5): p. 213, pl. 107, figs 38–39	21–21.5	3.7–4	21–22				x		
Navicymbula pusilla (Grunow) krammer	Fig. 4N	Lange-Bertalot et al. 2017: p. 417, pl. 90, figs 30–34	14–38	4.5–5.5	16–18				x	x	x
Rhoicosphenia abbreviata (C.Agardh) Lange-Bertalot	Fig. 4Q-T	Lange-Bertalot et al. 2017: p. 535, pl. 19, figs 43–49	17–44	5–8	14–17				x		x
Seminavis strigosa (Hustedt) Danieledis & Economou-Amilli	Fig. 4L,M	Al-Handal & Al-Shaheen 2019: p. 88, pl. 32, fig. 12; Lange-Bertalot et al. 2017: p. 335, pl. 94, figs 29–30	21–32	5–5.5	18–19			x	x	x	x
Amphipleura pellucida (Kützing) Kützing	Fig. 7C	Lange-Bertalot et al. 2017: p. 97, pl. 68, figs 27–29	74–93	7.5–8.8							x
Anomoeoneis sphaerophora Pfitzer	Fig. 8T	Al-Handal & Al-Shaheen 2019: p. 34, pl. 10, figs 4–5; Lange-Bertalot et al. 2017: p. 107, pl. 68, fig. 26	60–70	17.7–22	15–17					x	x
Brachysira neoexilis Lange-Bertalot	(*), Fig. 8F	Lange-Bertalot et al. 2017: p. 117, pl. 60, figs 9–10	15–30	4.8–5					x	x	x
Brachysira cf. *neoexilis* Lange-Bertalot	Fig. 8G	Lange-Bertalot et al. 2017: p. 117, pl. 60, figs 9–10	22–27	5.5–7						x	x
Berkeleya rutilans (Trentepohl ex Roth) Grunow	(r)	Witkowski et al. 2000: p. 157, pl. 62, figs 14–17	23–23.5	4–4.2							x
Berkeleya sp. 1	Fig. 8L		23.8–25.8	2.5–3							x

Taxa, Author		Reference	L	W	S	F	D	TS	TW	ES	EW
Caloneis permagna (Bailey) Cleve	(r)	Al-Handal & Al-Shaheen 2019: p. 67, pl. 23, figs 4–5	82–118	30–83	12–14				x		x
Caloneis australis Zidarova, Kopalová & Van de Vijver	(*), Fig. 8R	Zidarova et al. 2016 (b): p. 40, figs 1–17	24–53	5–7.5	18–21				x	x	x
Caloneis silicula (Ehrenberg) Cleve	Fig. 8S	Lange-Bertalot et al. 2017: p.125, pl. 70, figs 1–4	48–65(98)	11.5–15.6	16–17						x
Caloneis schumanniana (Ehrenberg) Cleve	(r)	Lange-Bertalot et al. 2017: p.125, pl. 70, figs 5–6	44–45	13–13.2	17–18						x
Caloneis sp. 1	(r)		22.3–24	5–5.1	17–18						x
Chamaepinnularia submuscicola (Krasske) Lange-Bertalot	(*), Fig. 8C	Lange-Bertalot et al. 2017: p.135, pl. 51, figs 31–36	9–11	2.9–3	19–20					x	
Craticula halophila (Grunow) D.G.Mann	Fig. 7F	Al-Handal & Al-Shaheen 2019: p. 82, pl. 30, figs 3–4; Lange-Bertalot et al. 2017: p. 147, pl. 45, fig. 9	55–90.1	12.2–15.7	18–19					x	x
Craticula buderi (Hustedt) Lange-Bertalot	(r)	Lange-Bertalot et al. 2017: p. 145, pl. 46, fig. 6	25–32	7–8.5	19–21			x			
Craticula cf. *subminuscula* (Manguin) C.E.Wetzel & Ector	Fig. 8A	Lange-Bertalot et al. 2017: p. 148, pl. 46, figs 21–26	9–6-10.8	4.5–5				x		x	
Craticula sp.1	(r)		30–31.5	6.8–7	13–14					x	
Diploneis sp. 1	Fig. 9R, S		10–26	9–14.5	12–14				x	x	x
Diploneis sp. 2	Fig. 9U		19–20	9.6–10	13–14			x			
Diploneis sp. 3	Fig. 9P		33–45	12–16	11–12				x	x	x
Diploneis sp. 4	Fig. 9Q		25–39	11–11.5	13–17						x
Diploneis sp. 5	Fig. 9T		18–22	10–11.5	13–14				x	x	x
Envekadea hedinii (Hustedt) Van de Vijver	Fig. 8H, I	Al-Handal & Al-Shaheen 2019: p. 68, pl. 24, figs 6–7	25–45.5	5.5–7	24–26				x	x	x
Fallacia pygmaea ssp. *subpygmaea* Lange-Bertalot et al.	(*), Fig. 8E	Lange-Bertalot et al. 2017: p. 263, pl. 47, figs 32–34	16–18	6.9–7				x			
Fallacia pygmaea (Kützing) Stickle & D.G.Mann cf. ssp. *pygmaea*	(r)	Lange-Bertalot et al. 2017: p. 262, pl. 47, figs 28–31	19–19.7	8–8.5	25–26					x	
Gyrosigma acuminatum (Kützing) Rabenhorst	Fig. 6C	Al-Handal & Al-Shaheen 2019: p. 77, pl. 26, figs 11–12	165–168.5	26–27		10–11			x		
Gyrosigma cf. *kuetzingii* (Grunow) Cleve	Fig. 7A	Lange-Bertalot et al. 2017: p. 328, pl. 64, figs 1–3	49–85	8–12		24–25		x	x		x
Gyrosigma parkeri (M.B.Harrison) Elmore	(r)		74–85	14.15				x		x	
Gyrosigma cf. *sciotoense* (W.S.Sullivant) Cleve	Fig. 6E	Lange-Bertalot et al. 2017: p. 329, pl. 64, figs 4–8	71–109	12.8–14				x	x		
Gyrosigma cf. *scalproides* (Rabenhorst) Cleve	Fig. 7B	Lange-Bertalot et al. 2017: p. 329, pl. 64, figs 4–8	80–81	12–13					x		
Gyrosigma sp. 1	Fig. 6F		44–69	5–12				x	x		
Gyrosigma sp. 2	Fig. 6D		117–120	16.5–17						x	x
Gyrosigma sp. 3	(r)		112	11.7					x		
Gyrosigma obtusatum	(r), (*)										
Haslea spicula (Hickie) Bukhtiyarova	Fig. 7D	Lange-Bertalot 2001 (V2): p. 160; pl. 125, figs 3–10; Al-Handal & Al-Shaheen 2019: p. 70, pl. 24, fig. 12	55–76	8–9.5						x	x
Hippodonta capitata (Ehrenberg) Lange-Bertalot, Metzeltin & Witkowski	(r)	Al-Handal & Al-Shaheen 2019: p. 70, pl. 24, figs 13–14	17	5	12						x
Hippodonta hungarica (Grunow) Lange-Bertalot, Metzeltin & Witkowski	(r)	Al-Handal & Al-Shaheen 2019: p. 71, pl. 24, figs 15–16	12–13	5.5–5.8	10–11			x			
Hippodonta sp. 1	Fig. 8B		13.8–16.5	4.5–5	13–14				x		

Taxa, Author		Reference	L	W	S	F	D	TS	TW	ES	EW
Luticola nivalis (Ehrenberg) D.G.Mann	Fig. 8K	Levkov et al. 2013 (V7): p. 175, pl. 177, figs 28,29; Lange-Bertalot et al. 2017: p. 357, pl. 46, Figs 54–58	18–19	6.9–7.6	19–20				x		
Luticola ventriconfusa Lange-Bertalot	(*), Fig. 8J	Levkov et al. 2013 (V7): p. 250, pl. 190, figs 34–37; Lange-Bertalot et al. 2017: p. 358, pl. 46, figs 49–50	12.5–15	6.5–7.5	19–20				x		
Luticola saprophila Levkov, Metzeltin & A.Pavlov	(r), (*)	Levkov et al. 2013 (V7): p. 213, pl. 77, figs 23–26	30–30.5	8–8.6	20–21					x	
Luticola paramutica (W.Bock) D.G.Mann	(r), (*)	Levkov et al. 2013 (V7): p. 182, pl. 12, fig. 18	19–19.7	5–5.6	21–22					x	
Luticola cf. *pseudolacertosa* (Cholnoky) Levkov, Metzeltin & A.Pavlov	(r), (*)	Levkov et al. 2013 (V7): p. 195, pl. 105, fig. 27	15–16	6–6.5	16–17					x	
Luticola sp. 1	(r)		20	6.5	13					x	
Mastogloia cf. *smithii* Grunow	Fig. 9H, I	Witkowski et al. 2000: p. 239, pl. 74, figs 13–16	25–51	10–11.5	16–18				x	x	x
Mastogloia smithii Thwaites ex W.Smith	Fig. 9J, K	Al-Handal & Al-Shaheen 2019: p. 33, pl. 9, figs 11, 12; Witkowski et al. 2000: p. 262, pl. 74, figs 3,4	35–38	11–11.7	18–19					x	x
Mastogloia elliptica (C.Agardh) Cleve	Fig. 9O	Al-Handal & Al-Shaheen 2019: p. 31, pl. 9, figs 3,4; Witkowski et al. 2000: p. 245, pl. 83, figs 15,16	20.47	9–12	16–18				x	x	x
Mastogloia lacustris (Grunow) Grunow	Fig. 9E, F	Al-Handal & Al-Shaheen 2019: p. 31, pl. 9, figs 5, 6	51–53	10–10.8	17.1				x		x
Mastogloia cf. *brunii* E.J.F.Wood	Fig. 9A, B	Al-Handal and Al-Shaheen 2019: p. 31, pl. 9, figs 1,2	35–55	13–17	15–17					x	x
"Mastogloia aff. *smithii* 1"	Fig. 9G	Lee et al. 2014: p. 346, fig. 76	42–54	12–13	18–19					x	
Mastogloia sterijovskii A.Pavlov, Jovanovska, C.E.Wetzel, Ector & Levkov	(*), Fig. 9L	Pavlov et al. 2016: p. 106, figs 240–289	26–32	10–10.5	18–20					x	x
Mastogloia belaensis Voigt	Fig. 9C, D	Van de vijver et al. 2017: p. 7, figs 17–23	25–52	11.5–14.5	14–15				x	x	x
Mastogloia sp. 1	Fig. 9N		20–24	9–10	20–21					x	
Mastogloia sp. 2	Fig. 9M		16.6–25	8.5–10	20–22					x	
Mastogloia sp. 3	(r)		22–23	12–13	21–22					x	
Navicula cf. *cryptotenelloides* Lange-Bertalot	Fig. 8AQ	Lange-Bertalot et al. 2017: p. 388, pl. 33, figs 6–10	13–16	3.7–4	16–18			x	x		x
Navicula cryptotenella Lange-Bertalot	(*), Fig. 8AG	Lange-Bertalot 2001 (V2): p. 28, pl. 26, figs 17–32; Lange-Bertalot et al. 2017: p. 387, pl. 33, figs 1–3	22–30	6–6.5	14–15					x	x
Navicula cryptocephala Kützing	Fig. 8AI	Lange-Bertalot 2001 (V2): p. 27, pl. 17, figs 1–10	22.7–25	5–5.5	14			x			x
Navicula veneta Kützing	Fig. 8AM	Al-Handal & Al-Shaheen 2019: p. 75, pl. 26, fig. 4	18–23.5	5–5.5	14–15				x		x
Navicula cf. *veneta* Kützing	(r)	Lange-Bertalot et al. 2017: p. 412, pl. 32, figs 44–48	24–25	6–6.5	15–16						x
Navicula lundii E.Reichardt	(r), (*)	Lange-Bertalot 2001 (V2): p. 46, pl. 22, figs 17–24	22–22.5	5.6–6	14–15					x	
Navicula vandamii Schoeman & R.E.M.Archibald var. *vandamii*	Fig. 8AJ	Lange-Bertalot et al. 2017: p. 411, pl. 30, figs 15–19	24.8–26	5.4–5.7	15–16			x			
Navicula cf. *vandamii* var. *vandamii* Schoeman & R.E.M.Archibald	(r)	Lange-Bertalot et al. 2017: p. 411, pl. 30, figs 15–19	22–25	5–5.5	15			x			
Navicula gregaria Donkin	Fig. 8W	Lange-Bertalot 2001 (V2): p. 85, pl. 38, figs 8–18	24–31	6.5–7	15–16				x		
Navicula salinarum var. *rostellata* (Hustedt) Lange-Bertalot	(*), Fig. 8AH	Witkowski et al. 2000: p. 304, pl. 123, figs 9–14	21–25	7–7.5	13–17			x			
Navicula cf. *praeterita* Hustedt	(r)	Lange-Bertalot 2001 (V2): p. 85, pl. 10, figs 1–7	31–31.5	7–7.5	13–14					x	
Navicula rostellata Kützing	Fig. 8AB	Lange-Bertalot et al. 2017: p. 404, pl. 38, figs 10–14	35–41	9–10	12–14			x	x	x	x
Navicula rhynchotella Lange-Bertalot	Fig. 8AC	Witkowski et al. 2000: p. 303, pl. 120, figs 11–15	38–44	13–14	9–10					x	x

Taxa, Author		Reference	L	W	S	F	D	TS	TW	ES	EW
Navicula cf. *margalithii* Lange-Bertalot	Fig. 8AE	Krammer & Lange-Bertalot 1991: p. 79, pl. 17, figs 1–3	40–54	8.5–9	11–13				x		x
Navicula recens (Lange-Bertalot) Lange-Bertalot	Fig. 8V	Lange-Bertalot 2001 (V2): p. 62, pl. 1, figs 16–22	18–40	7–8	11–12			x	x	x	x
Navicula phylleptosoma Lange-Bertalot	(*), Fig. 8AO	Witkowski et al. 2000: p. 299, pl. 122, figs 10–17	14.5–18.7	4.5–5	17–20				x		
Navicula phyllepta Kützing	(r), (*)	Lange-Bertalot 2001 (V2): p. 56, pl. 46, figs 1–9	25–26	6–6.5	17–18				x		
Navicula reichardtiana Lange-Bertalot, nom. illeg. non (Grunow) Migula ≡ *Navicula metareichardtiana* Lange-Bertalot & Kusber	(*), Fig. 8AR	Lange-Bertalot 2001 (V2): p. 63, pl. 13, figs 25–35	10–13	4–4.8	14–16					x	
"*Navicula* spec. cf. *salinicola* Hustedt"	Fig. 8AL	Witkowski et al. 2000: p. 304, pl. 125, figs 9–11	14.5–21	4–4-5	14–16				x		
Navicula wildii Lange-Bertalot	(*), Fig. 8AD	Lange-Bertalot et al. 2017: p. 416, pl. 36, figs 6–10	27–44	6–7.5	11.5–12				x	x	x
Navicula escambia (R.M.Patrick) Metzeltin & Lange-Bertalot	(*), Fig. 8AA	Lange-Bertalot et al. 2017: p. 391, pl. 39, figs 1–5	27–47	6.5–8.8	13–14			x	x		
Navicula erifuga Lange-Bertalot	Fig. 8X	Lange-Bertalot et al. 2017: p. 390, pl. 39, figs 12–16	25–32	5–6.5	12–14			x	x	x	x
Navicula simulata Manguin	(*), Fig. 8AF	Lange-Bertalot et al. 2017: p. 406, pl. 39, figs 6–11	29–39	6–8	14–16			x	x	x	x
Navicula torganae Metzeltin, Lange-Bertalot & García-Rodríguez	(r), (*)	Metzeltin 2005: p. 148, pl. 49	27–28	8.8–9	13–14						x
Navicula cf. *torganae* Metzeltin, Lange-Bertalot & García-Rodríguez	(r)	Metzeltin 2005: p. 148, pl. 49	17.5–19	6–7	15–16					x	
Navicula tripunctata (O.F.Müller) Bory	(r)	Lange-Bertalot 2001 (V2): p. 73, pl. 1, figs 1–8	46.5–50	7–7.5	10–11					x	x
Navicula cf. *subagnita* Proshkina-Lavrenko	Fig. 8Y	Witkowski et al. 2000: p. 308, pl. 131, figs 15–19	32.5–38	5–6	15–17					x	x
Navicula sp. 1	(r)		21.7–25	3.7–4.5	14–16					x	x
Navicula sp. 2	(r)		13–16	3.5–3.7	18–20					x	
Navicula sp. 3	Fig. 8Z		35–37	5.7–6	16–17					x	
Navicula sp. 4	Fig. 8AK		21.5–23	5–5.5	19–20			x			
Navicula sp. 5	(r)		2122	4.5–4.7	18–20			x		x	
Navicula sp. 6	Fig. 8AN									x	
Navicula sp. 7	(r)		28–30	7.5–8	14–15			x			
Navicula sp. 8	Fig. 8AP		16–21	5–6.5	17–18					x	
Parlibellus crucicula (W.Smith) Witkowski, Lange-Bertalot & Metzeltin	Fig. 7E	Witkowski et al. 2000: p. 321, pl. 103, figs 11–13	35–64	14–19	18–19			x			
Pinnularia appendiculata var. *amaniana* krammer	(r), (*)	Krammer 2000 (V1): p. 121, pl. 91, figs 10–11	16–23	4–4.8	17–18					x	
Pleurosigma angulatum (J.T.Quekett) W.Smith	(r)	Al-Handal & Al-Shaheen 2019: p. 80, pl. 29, fig. 1	77–93	13–15						x	
Pleurosigma sp. 1	Fig. 6B		77–87.5	12–14.5				x		x	x
Pleurosigma sp. 2	(r)		200–202	20–21	10–11					x	
Pleurosigma sp. 3	Fig. 6A		140–144	15–16	12–13					x	
Prestauroneis furatensis H.Mohamad et N.Abarca	Fig. 8O	Mohamad et al. accepted	24.5–19	7.9–9.5	16–20					x	
Prestauroneis sp.1	Fig. 8M		17–22	5–6	20–21					x	
Prestauroneis sp.2	Fig. 8N		33–34.5	10.5–11.5	23.24					x	
Prestauroneis sp.3	(r)		27–28	7–7.7	20–22				x		

Taxa, Author		Reference	L	W	S	F	D	TS	TW	ES	EW
Pseudofallacia cf. *tenera* (Hustedt) Y.Liu, Kociolek & Q.Wang	Fig. 8D	Lange-Bertalot et al. 2017: p. 529, pl. 47, figs 35–38; Al-Handal & Al-Shaheen 2019: p. 60, pl. 19, fig. 17	9.3–13	6–6.8	27–18					x	
Pseudofallacia sp.1	(r)		13–14	4–4.8	18–19					x	
Stauroneis sp.	(r)		28.5	6	18					x	
Scoliopleura basrensis Al-Handal & Pennesi	Fig. 8U	Al-Handal & Al-Shaheen 2019: p. 57, pl. 18, figs 6–11	28–32	7.5–8	26–28			x		x	
Sellaphora Pupula (Kützing) Mereschkovsky	(r)	Al-Handal & Al-Shaheen 2019: p. 60, pl. 19, figs 14–16; Lange-Bertalot et al. 2017: p. 544, pl. 42, figs 6–14	27–30	7–8	12–13					x	x
Sellaphora cf. *pupula* (Kützing) Mereschkovsky	(r)	Al-Handal & Al-Shaheen 2019: p. 60, pl. 19, figs 14–16; Lange-Bertalot et al. 2017: p. 544, pl. 42, figs 6–14	46	10	18					x	
Sellaphora pseudopupula (Krasske) Lange-Bertalot	(r), (*)	Lange-Bertalot et al. 2017: p. 547, pl. 43, figs 5–11	23–26	7–8	21–22					x	
EPITHEMIOID											
Epithemia adnata (Kützing) Brébisson	Fig. 11U, V	Lange-Bertalot et al. 2017: p. 218, pl. 121, figs 5–9	32–69	10–12	11–12				x		x
Rhopalodia gibba (Ehrenberg) O.Müller	Fig. 11S, T	Al-Handal & Al-Shaheen 2019: p. 102, pl. 37, figs 9–11; Lange-Bertalot et al. 2017: p. 537, pl. 124, figs 35–38	35–170	7.5–12	6–8				x	x	x
NITZSCHIOID											
Bacillaria paxillifera (O.F.Müller) Hendey	Fig. 11A	Al-Handal & Al-Shaheen 2019: p. 88, pl. 32, figs 13–15; Lange-Bertalot et al. 2017: p. 109, pl. 120, figs 1–5	64.5–101.5	5.5–6.5	23–24			x	x	x	x
Hantzschia amphioxys (Ehrenberg) Grunow	(r)	Lange-Bertalot et al. 2017: p. 338, pl. 104, figs 1–5; Al-Handal & Al-Shaheen 2019: p. 89, pl. 33, fig. 1	36–36.5	6–6.5	24–25					x	
Nitzschia dubia W.Smith	(r)	Al-Handal & Al-Shaheen 2019: p. 93, pl. 43, fig. 1	108–110	12–13	21–22				x		
Nitzschia microcephala Grunow	(r)	Witkowski et al. 2000: pl. 208, figs 5–11; Lange-Bertalot et al. 2017: p. 453, pl. 113, figs 41–47	8–12	3–3.5		14–15				x	
Nitzschia elegantula Grunow	Fig. 10AD	Al-Handal & Al-Shaheen 2019: p. 93, pl. 43, figs 2–4	10–17.5	3–3.8		12–14				x	x
Nitzschia filiformis (W.Smith) Van Heurck	Fig. 10G	Lange-Bertalot et al. 2017: p. 442, pl. 118; Al-Handal Krammer Al-Shaheen 2019: p. 94, pl. 34, figs 6–9	44–80	4.5		7–9		x	x	x	
Nitzschia cf. *filiformis* (W.Smith) Van Heurck	(r)	Lange-Bertalot et al. 2017: p. 442, pl. 118; Al-Handal Krammer Al-Shaheen 2019: p. 94, pl. 34, figs 6–9	108–109	5–5.5		8–9		x			
Nitzschia filiformis var. *conferta* (P.G.Richter) Lange-Bertalot	(*), Fig. 10M	Lange-Bertalot et al. 2017: p. 443, pl. 118, Figs 7–12; Krammer & Lange-Bertalot 1988 (2/2): p. 28, pl. 20, figs 1–7	27–38	4–6		9–12		x		x	
Nitzschia gracilis Hantzsch	Fig. 10F	Lange-Bertalot et al. 2017: p. 446, pl. 109, figs 10–14; Krammer & Lange-Bertalot 1988 (2/2): p. 348, pl. 66, figs 1–11	45–78	3.8–4		12–13				x	
Nitzschia cf. *gracilis* Hantzsch	(r)	Lange-Bertalot et al. 2017: p. 446, pl. 109, Figs 10–14; Krammer & Lange-Bertalot 1988 (2/2), p. 348, pl. 66, figs 1–11	34–45	4–4.5		12–13		x			
Nitzschia clausii Hantzsch	Fig. 10H	Lange-Bertalot et al. 2017: p. 438, pl. 118, figs 15–18; Al-Handal & Al-Shaheen 2019: p. 92, pl. 33, figs 19–20	34–60	3.8–5		9–10		x	x	x	x
Nitzschia cf. *clausii* Hantzsch	Fig. 10O	Lange-Bertalot et al. 2017: p. 438, pl. 118, figs 15–18; Al-Handal & Al-Shaheen 2019: p. 92, pl. 33, figs 19–20	18.5–31.5	4–4.8		9–12		x		x	
Nitzschia cf. *heufleriana* Grunow	Fig. 10D	Lange-Bertalot et al. 2017: p. 447, pl. 111, figs 19–23	88–122	5.8–7		10–11			x		
Nitzschia dissipata (Kützing) Grunow ssp. *dissipata*	(r)	Lange-Bertalot et al. 2017: p. 440, pl. 111, figs 8,10	39.5–57.5	4.2–4.5		7–10			x		

Taxa, Author		Reference	L	W	S	F	D	TS	TW	ES	EW
Nitzschia dissipata (Kützing) Rabenhorst	Fig. 10T	Al-Handal & Al-Shaheen 2019: p. 93, pl. 33, figs 22–24	(24) 29.7–33	4.5–5		8–9			x		
Nitzschia palea (Kützing) W.Smith	Fig. 10J	Al-Handal & Al-Shaheen 2019: p. 96, pl. 34, figs 17–18	24–85	3.5–5		11–14		x		x	
Nitzschia cf. *palea* (Kützing) W.Smith	Fig. 10N	Al-Handal & Al-Shaheen 2019: p. 96, pl. 34, figs 17–18	32–35	5.7–6		11–12		x			
Nitzschia palea var. *debillis* (Kützing) W.Smith	(*), Fig. 10W	Lange-Bertalot et al. 2017: p. 452, pl. 113, figs 17–20	22–30	3–3.8		12–15		x		x	
Nitzschia cf. *palea* var. *debillis* (Kützing) W.Smith	Fig. 10X	Lange-Bertalot et al. 2017: p. 452, pl. 113, figs 17–20	26.5–27	4		13		x		x	
Nitzschia paleacea (Grunow) Grunow	Fig. 10U	Lange-Bertalot et al. 2017: p. 453, pl. 113, figs 21–29	30–31	2.9–3		14–15		x			
Nitzschia capitellata Hustedt	(r)	Lange-Bertalot et al. 2017: p. 438, pl. 115, figs 11–16; Al-Handal & Al-Shaheen 2019: p. 92, pl. 33, figs 17–18	38–54	4.5–5		12–13					x
Nitzschia reversa W.Smith	Fig. 10E	Krammer & Lange-Bertalot 1988 (2/2): p. 124, pl. 85, figs 7–10	70–100	4–4.5		12–14		x		x	
Nitzschia vitrea G.Norman var. *vitrea*	(r)	Krammer & Lange-Bertalot 1988 (2/2): p. 73, pl. 65, figs 1,2	49–50.5	7–8		5–6			x		x
Nitzschia sigma (Kützing) W.Smith	Fig. 10A	Al-Handal & Al-Shaheen 2019: p. 97, pl. 35, figs 6–7; Lange-Bertalot et al. 2017: p. 456, pl. 117, figs 7–11	75–116	7–7.8		8–9		x		x	
Nitzschia intermedia Hantzsch ex Cleve & Grunow	Fig. 10C	Lange-Bertalot et al. 2017: p. 448, pl. 109, figs 1–6	79.5–110	5.8–6		9–10				x	
Nitzschia umbonata (Ehrenberg) Lange-Bertalot	(r)	Lange-Bertalot et al. 2017: p. 463, pl. 107, figs 1–2	55–56	5–6		9–10		x			
Nitzschia cf. *acicularioides* Hustedt	Fig. 10I	Krammer & Lange-Bertalot 1988 (2/2): p. 118, pl. 67, figs 1, 2	46–88	3–3.5		12–13		x		x	
Nitzschia cf. *kurzeana* Rabenhorst	Fig. 10B	Al-Handal & Al-Shaheen 2019: p. 95, pl. 34, figs 2, 3	62–105	7–8.5		7–8		x	x	x	x
Nitzschia cf. *obtusa* W.Smith	(r)	Al-Handal & Al-Shaheen 2019: p. 95, pl. 35, figs 2, 3	80–171	8–9		5–6				x	x
Nitzschia amphibia Grunow	Fig. 10AC	Lange-Bertalot et al. 2017: p. 435, pl. 119, figs 9–15	15–35	4.8–5	16–18				x	x	x
Nitzschia bulnheimiana (Rabenhorst) H.L.Smith	(*), Fig. 10AG	Lange-Bertalot et al. 2017: p. 437, pl. 114, figs 40–43	12–20	3.5–4	10–12			x		x	
Nitzschia dealpina Lange-Bertalot & G.Hofmann	(*), Fig. 10Q	Lange-Bertalot et al. 2017: p. 439, pl. 110, figs 16–21	8–12.5	3.5–3.7	22	14		x			
Nitzschia sp.1	Fig. 10L		35–44.4	2.8–4.2				x		x	
Nitzschia sp. 2	(r)		37–79	2.8–4	13–15					x	
Nitzschia sp. 3	(r)		75	5	16	7			x		
Nitzschia sp. 4	Fig. 10AA		20–21	4.8–5		12–13		x			
Nitzschia sp. 5	Fig. 10Z		11–12	3–3.5		13–14				x	
Nitzschia sp. 6	Fig. 10R		11–15.5	3.5–3.8	22–23	12–13		x			
Nitzschia sp. 7	Fig. 10AF		34–66	4–5		16–17				x	x
Nitzschia sp. 8	Fig. 10K		35–66	4–5	16–18	11–13		x		x	x
Nitzschia sp. 9	Fig. 10AB		16–35	4–4.5	17–18	12–13		x		x	x
Nitzschia sp. 10	Fig. 10Y		17–30	3.8–5	17–19	12–14				x	
Nitzschia cf. *frustulum* (Kützing) Grunow	Fig. 10AE	Lange-Bertalot et al. 2017: p. 444, pl. 114, figs 28–30	14–20	2–2.5		12–14			x		
Nitzschia inconspicua Grunow	Fig. 10S	Lange-Bertalot et al. 2017: p. 444, pl. 114, figs 31–34	7–11	2.5–2.8		15–16		x	x		
Nitzschia hantzschiana Rabenhorst	Fig. 10V	Lange-Bertalot et al. 2017: p. 437, pl. 114, figs 55–59	21–33	3–3.5	23–24	11–12		x		x	
Nitzschia cf. *solita* Hustedt	Fig. 10P	Lange-Bertalot et al. 2017: p. 459, pl. 114, figs 16–20	16–25	4.8–5		13–15		x		x	
Nitzschia liebethruthii Rabenhorst	(r)	Lange-Bertalot et al. 2017: p. 449, pl. 110, figs 39–45	8–12.5	3–3.6		12–14		x			
Nitzschia permiuta Grunow	(r)	Lange-Bertalot et al. 2017: p. 453, pl. 114, figs 49–54	19	3.4	23	12				x	

Taxa, Author		Reference	L	W	S	F	D	TS	TW	ES	EW
Tryblionella angustata W.Smith	(*), Fig. 11C	Lange-Bertalot et al. 2017: p. 595, pl. 106, figs 13–17	40.5–45	6.6–7	15–16				x		
Tryblionella angustatula (Lange-Bertalot) Cantonati & Lange-Bertalot	Fig. 11K	Lange-Bertalot et al. 2017: p. 596, pl. 106, figs 8–12	13–24	4–4.5	16–18					x	
Tryblionella cf. *angustatula* (Lange-Bertalot) Cantonati & Lange-Bertalot	(r)	Lange-Bertalot et al. 2017: p. 596, pl. 106, figs 8–12	10–11.5	3.8–4	17–18					x	
Tryblionella apiculata W.Gregory	(r)	Lange-Bertalot et al. 2017: p. 596, pl. 106, figs 18–22	30–41	4.7–6	15–16			x	x		x
Tryblionella calida Grunow	Fig. 11D	Lange-Bertalot et al. 2017: p. 597, pl. 105, figs 5–8	27.5–63	7–8	32–33			x	x	x	
Tryblionella compressa (Bailey) Poulin	Fig. 11H	Krammer & Lange-Bertalot 1988 (2/2): p. 46, pl. 37, figs 1–5	13–22	7–9	12–14			x	x		x
Tryblionella compressa var. *balatonis* (Grunow) Lange-Bertalot	Fig. 11I	Krammer & Lange-Bertalot 1988 (2/2): p. 46, pl. 38, figs 1–4	17–24	7–7.5	16–17			x		x	
Tryblionella cf. *coarctata* (Grunow) D.G. Mann	(r)	Witkowski et al. 2000: pl. 186, fig. 5	24–25	10–10.5	18–19					x	
Tryblionella cf. *debillis* Arnott ex O'Meara	(r)	Witkowski et al. 2000: p. 377, pl. 185, figs 11–13	16.5–18.5	6.5–6.8	10–12			x			
Tryblionella granulata (Grunow) D.G.Mann	Fig. 11F	Al-Handal & Al-Shaheen 2019: p. 99, pl. 35, fig. 14; Witkowski et al. 2000: p. 384, pl. 189, figs 1–5	27–31.5	13–14.5	6–7						x
Tryblionella hungarica (Grunow) Frenguelli	Fig. 11B	Lange-Bertalot et al. 2017: p. 598, pl. 106, figs 3–7; Al-Handal & Al-Shaheen 2019: p. 100, pl. 36, fig. 4	40–112	5.5–8	16–17				x	x	x
Tryblionella levidensis W.Smith	Fig. 11E	Al-Handal & Al-Shaheen 2019: p. 100, pl. 36, figs 5–7; Lange-Bertalot et al. 2017: p. 599, pl. 105, figs 1–4	30–34.6	15.5–17.5	7–7.5			x	x		
Tryblionella sp. 1	Fig. 11J		9–13	3.8–4	18–20					x	
Tryblionella sp. 2	(r)		32–38	7.5–7.7	12–13				x	x	
Tryblionella sp. 3	Fig. 11G		23–25	9–9.5	18–20					x	
SURIRELLOID											
Entomoneis cf. *paludosa* (W.Smith) Reimer	Fig. 11R	Lange-Bertalot et al. 2017: p. 216, pl. 133, figs 13–15; Al-Handal & Al-Shaheen 2019: p. 103, pl. 38, figs 1–2	25–35	5.5–7				x			
Entomoneis paludosa (W.Smith) Reimer	(r)	Al-Handal & Al-Shaheen 2019: p. 103, pl. 38, figs 1–2	38–43	6–7	24–25					x	x
Iconella curvula (W.Smith) Ruck & Nakov	(r)	Al-Handal & Al-Shaheen 2019: p. 105, pl. 40, fig. 4	91–92	5–6	very fine						x
Surirella angusta Kützing	(r)	Lange-Bertalot et al. 2017: p. 582, pl. 133, figs 1–5	35.8–39	8–9	7–7.5				x		
Surirella brebissonii var. *kuetzingii* Krmmer et Lange-Bertalot	Fig. 11O	Lange-Bertalot et al. 2017: p.584, pl. 132, figs 17–21	21.4–27	13.5–15					x		
Surirella brightwellii W.Smith	Fig. 11M	Krammer & Lange-Bertalot 1988: p. 183, pl. 132, fig. 3	56	24–30–7							x
Surirella librile (Ehrenberg) Ehrenberg	Fig. 11P, Q	Al-Handal & Al-Shaheen 2019: p. 107, Pl. 40, fig. 3.4	42–93	13–16.5	8–9				x		
Surirella neglecta E.Reichardt	Fig. 11N	Reichardt 2018: pl. 423	20–29	10.9–12					x		
Surirella robusta Ehrenberg ≡ *Iconella robusta* (Ehrenberg) Ruck & Nakov	(r)	Al-Handal & Al-Shaheen 2019: p. 108, pl. 42, fig. 2; Lange-Bertalot et al. 2017: p. 587, pl. 129, figs 1–2	143.2	54.2		3					x
Surirella splendida (Ehrenberg) Kützing ≡ *Iconella splendida* (Ehrenberg) Ruck & Nakov	(r)	Al-Handal & Al-Shaheen 2019: p. 108, pl. 42, fig. 1; Krammer & Lange-Bertalot 1988: p. 202, pl. 158, figs 1–3	123–130	35.5–38		1.5–2				x	
Surirella striatula Turpin	Fig. 11L	Al-Shaheen 2016: p. 159, pl. 22, fig. 9	41.7–72.6	22–32.5	15–16			x	x	x	x
Surirella suecica Grunow	(r)	Reichardt 2018: p. 246, pl. 424	10.5–11.5	5-.52				x			
Surirella cf. *suecica* Grunow	(r)	Reichardt 2018: p. 246, pl. 424	10.7–14	5.3–5.4				x			

Bioinformatics analysis

Samples have been demultiplexed and split into individual per-sample Fastq files, one corresponding to the forward reads (R1) and one to the reverse reads (R2). Then we conducted bioinformatic analyses on them to generate the Amplicon Sequence Variants (ASVs) that constituted the fundamental units on which further examinations were carried out. The DIV4for and DIV4rev primers from all the demultiplexed MiSeq reads were removed by cutadapt (Martin, 2011). ASVs were generated using the R package DADA2 (Callahan et al. 2016) after processing the resulting R1 and R2 reads together. Where the R1 and R2 reads were truncated at R1 to 220 bp and at R2 to 170 nucleotides, based on their quality profiles (median quality score < 30), and those reads with ambiguities or showing an expected error (maxEE) higher than 2 were removed. The DADA2 denoising algorithm was then applied to determine an error rates model in order to infer amplicon sequence variants (ASVs). Finally, ASVs detected as chimeras were discarded using the DADA2 function “removeBimeraDenovo”.

Taxonomic assignment was performed using an own established reference library comprising the Diat.barcode library (Rimet et al. 2019) and the reference library of the Diatom research group of the Botanic Garden Berlin (5768 taxa for 18SV4). Relative read abundances of taxa were then calculated and used in subsequent analyses.

Following the bioinformatic analyses conducted with DADA2, the R package metabaR was employed to detect and identify artefactual sequences, such as contaminants and tag-jumps (Zinger et al. 2021). The dataset underwent a thorough examination to identify dysfunctional PCRs based on PCR replicates similarities. Subsequently, the reads from replicates were aggregated.

Data analysis

For assessing the effectiveness of the two methods in identifying taxa, the percentages of species and genera recorded molecularly and morphologically were calculated (relative abundances ≥ 1%). Data processing, visualizations and statistical analysis were performed in R version 4.2.0. Alpha Diversity Indices, including taxa richness and the Shannon Diversity Index, were computed using the vegan 2.6 R package (Oksanen et al. 2022). Variations in community structure between samples collected from the Euphrates and Tigris Rivers during summer 2019 and winter 2020 were assessed using both metabarcoding and morphology data. The Bray-Curtis Dissimilarity Measure, implemented through phyloseq, was employed to quantify dissimilarities (to study the pattern of diatom assemblages), which were then visualized using Non-metric Multidimensional Scaling (NMDS) ordination.

Permutational multivariate analysis of variance (PERMANOVA) was used to evaluate the statistically significant differences in diatom community composition regarding location and season for the DNA metabarcoding and the LM dataset. For the PERMANOVA analyses the R package vegan was used.

Venn diagrams with Eulerr (Larsson 2021) were used to compare the number of species present in the summer and winter for both rivers as well as between the two rivers, based on DNA metabarcoding and the LM dataset. Barplot diagrams at the genus level were generated for both metabarcoding and morphology data using the R package phyloseq (McMurdie and Holmes 2013).

Results

Morphological analysis

A total of 181 diatom species were identified (relative abundances ≥ 1%) (Figs 2–11). The additional 103 taxa were observed by scanning the whole slides looking for rare taxa, bringing the total diversity to 284 taxa belonging to 59 genera (Table 3). Notably, 46 species are recorded for the first time in the region and 62 others could not be identified to species level and are possibly new to science, as was the case with *Prestauroneis furatensis* H.Mohamad & N.Abarca, which was identified and described from the epiphytic community of the River Euphrates (Mohamad et al. in press).

The most common taxa (relative abundances ≥ 1%) across Tigris samples were in decreasing order: *Navicula recens* (33.3%), *Cocconeis placentula* complex (23.9%) and *Navicula rostellata* (15.4%). Across Euphrates samples the most abundant taxa were: *Cocconeis placentula* complex (81%), *Achnanthidium minutissimum* complex (62.1%) and *Encyonopsis* cf. *microcephala* (60.7%).

Table 2 presents a list of the physical and chemical composition of the water obtained from the sampling sites. The Euphrates generally exhibited higher values for conductivity, water temperature, silica, and transparency, while the Tigris had higher values for alkalinity, turbidity and nitrate.

Metabarcoding analysis

The Illumina MiSeq sequencing run generated 6,118,319 reads for the 18SV4 marker from 43 samples (Sample 10 at station E1 in summer, Samples 36 and 40 at station E2 in winter and Sample 24 at station T2 in winter were unsuccessful with PCR). After processing the reads through the DADA2 pipeline and improvement of the dataset by metbaR 5,461,214 reads remained belonging to 2,953 amplicon sequence variants (ASVs).

The total amount of reads was 5,461,214 with 1,454 (49.2%) of all ASVs classified as Bacillariophyta. The remaining were identified as 383 (12,9%) Chlorophyta, 36 (1,2) Ochrophyta, 2 (0.07%) Heterokontophyta and 1078 (36.5%) NA. Here again, the majority of the non-diatom reads were assigned to Chlorophyta. From 1,454 ASVs 408 could be assigned to a species in the reference database, whereby several ASVs were assigned to the same species (108). 959 ASVs were assigned to the genus level, whereby several ASVs were assigned to the same genus. The ASVs with the most reads, in decreasing order, belong to: *Navicula directa*, *Cocconeis placentula* complex, NA (Fragilariophyceae) and *Nitzschia palea*. The maximum number of ASVs per sample was 218 (in sample E 35) and the minimum 14 (in sample E 17).

Comparison of taxa detected by DNA metabarcoding and morphology

In most cases, metabarcoding analysis recovered more taxa than the morphological analysis. The metabarcoding analysis resulted in the identification of 1,454 ASVs, including 408 species with several ASVs belonging to the same taxa (108). Many species had no record in reference databases. Morphological analysis of environmental samples resulted in the identification of 284 taxa. At the genus level, 59 genera were recovered by morphology, whereas 54 genera were identified by metabarcoding analysis.

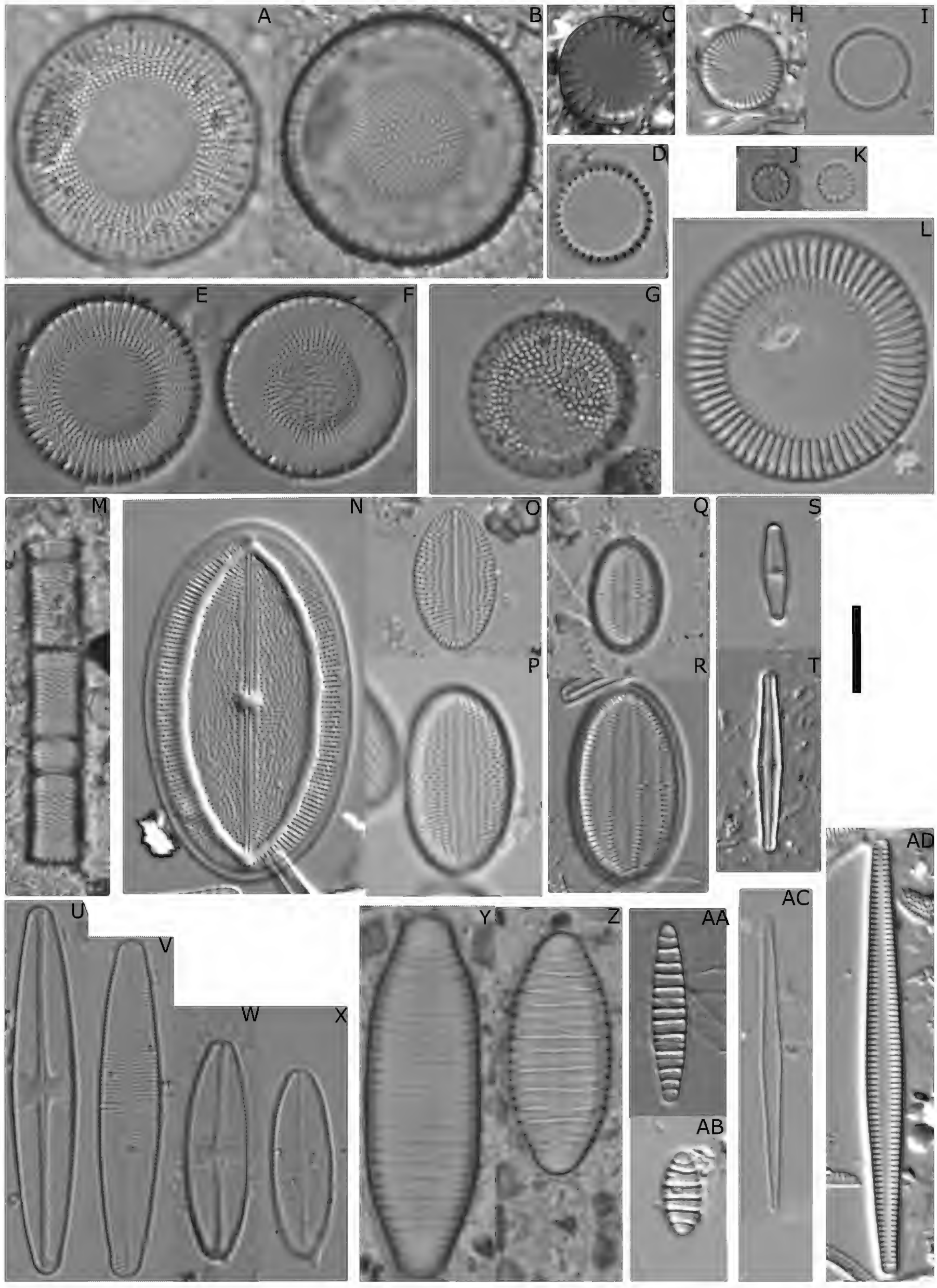

Figure 2. LM pictures of taxa found by morphological analyses. **A, B** *Stephanodiscus neoastraea*. **C** *S. hanztschii* var. *tenuis*. **D** *S. hanztschii* var. *hantzschii*. **E, F** *S. alpinus*. **G** *Thalassiosira lacustris*. **H, I** *Cyclostephanos invisitatus*. **J, K** *Cyclotella* sp. 1. **L** *C. meneghiniana*. **M** *Aulacoseira ambigua*. **N–P** *Cocconeis placentula* complex. **Q, R** *C. euglypta*. **S, T** *Achnanthidium minutissimum* complex. **U–X** *Lemnicola hungarica*. **Y, Z** *Diatoma vulgaris*. **AA, AB** *D. moniliformis*. **AC** *Synedropsis abuflosensis*. **AD** *Tabularia fasciculata*. Scale bar: 10 µm.

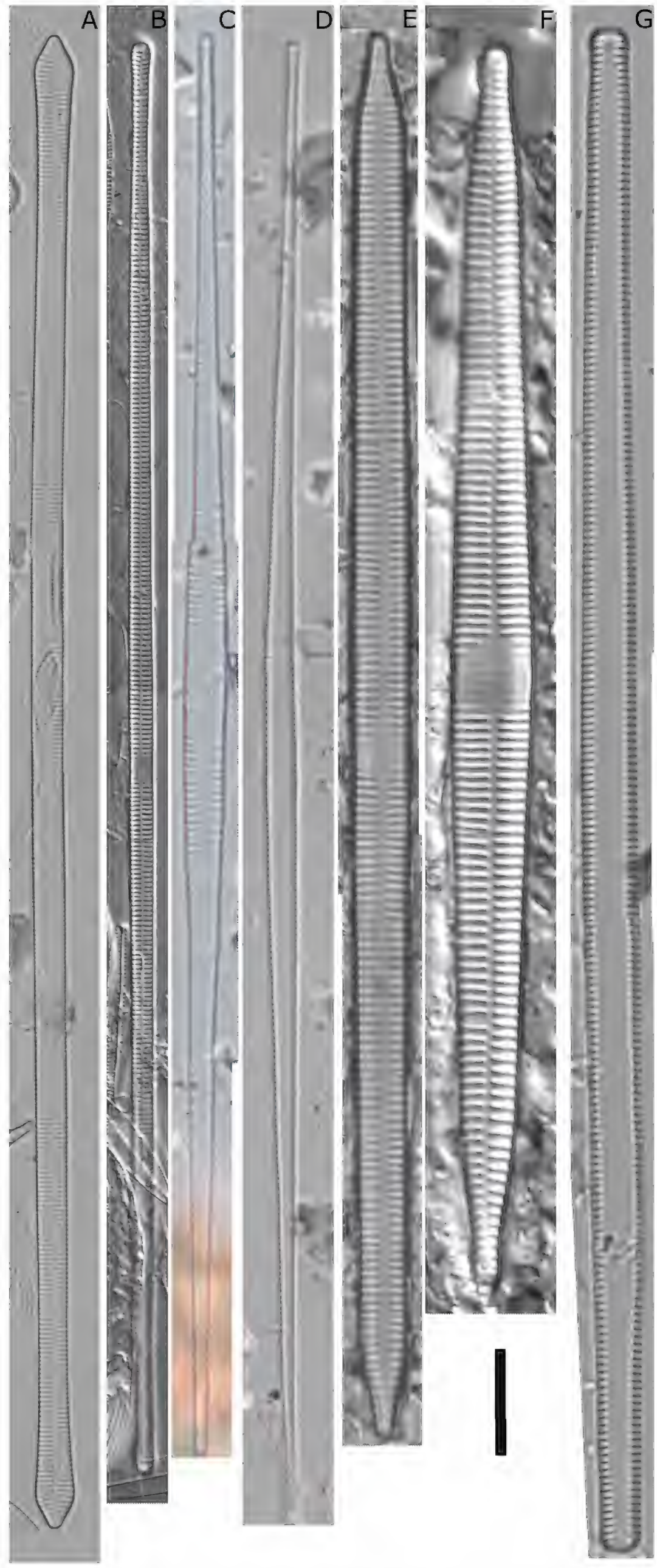

Figure 3. LM pictures of taxa found by morphological analyses. **A** *Ulnaria capitata*. **B** *U. danica*. **C** *U. acus*. **D** *U. delicatissima* var. *angustissima*. **E** *U. ulna* var. *claviceps*. **F** *U. ulna* var. *ulna*. **G** *Fragilaria koensabbei*. Scale bar: 10 µm.

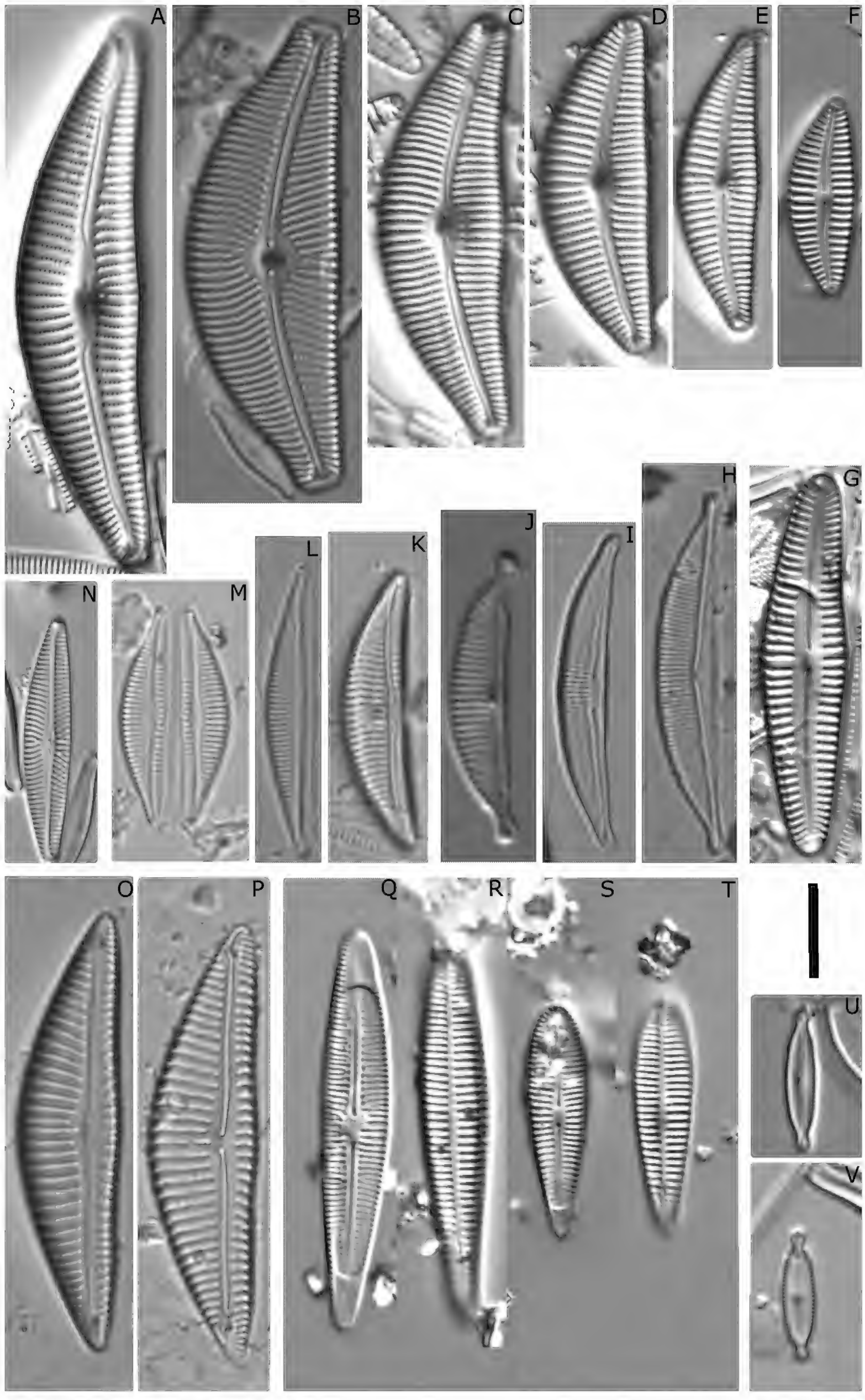

Figure 4. LM pictures of taxa found by morphological analyses. **A** *Cymbella cymbiformis*. **B** *C. tumida*. **C** *C. neocistula*. **D** *C.* cf. *cymbiformis*. **E** *C. sumatrensis*. **F** *C. hustedtii*. **G** *C. stigmaphora*. **H** *Halamphora* cf. *coffeiformis*. **I** *H. veneta*. **J** *H. coffeiformis*. **K** *Amphora copulata*. **L, M** *Seminavis strigose*. **N** *Navicymbula pusilla*. **O** *Encyonema vulgare* var. *vulgare*. **P** *E.* sp.1. **Q–T** *Rhoicosphenia abbreviata*. **U** *Encyonopsis* cf. *minuta*. **V** *E.* cf. *microcephala*. Scale bar: 10 µm.

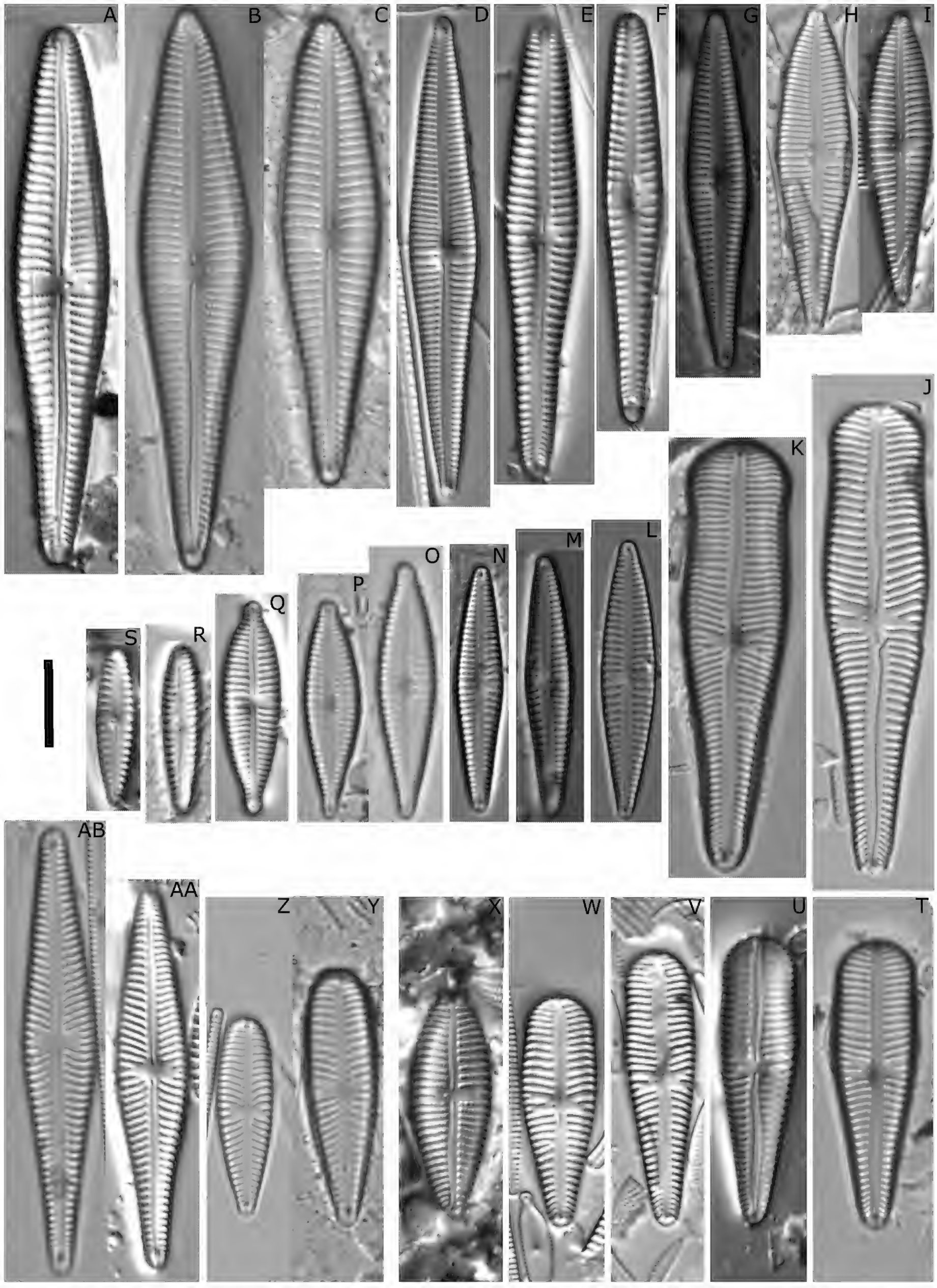

Figure 5. LM pictures of taxa found by morphological analyses. **A** *Gomphonema affine*. **B, C** *G.* cf. *affine*. **D** *G. naviculoides*. **E** *G.* cf. *subclavatum*. **F** *G. vibrio*. **G** *G.* cf. *hebridense*. **H, I** *G. pseudoaugur*. **J** *G.* cf. *laticollum*. **K** *G.* cf. *truncatum*. **L** *G. graciledictum*. **M** *G. hebridense*. **N** *G. auritum*. **O, P** *G. parvulum*. **Q** *G.* cf. *lagenula*. **R, S** *G. pumilum* var. *pumilum*. **T–W** *G. capitatum* complex. **X** *G.*cf. *pseudaffine*. **Y, Z** *Gomphonella olivacea*. **AA, AB** *G. coxiae*. Scale bar: 10 µm.

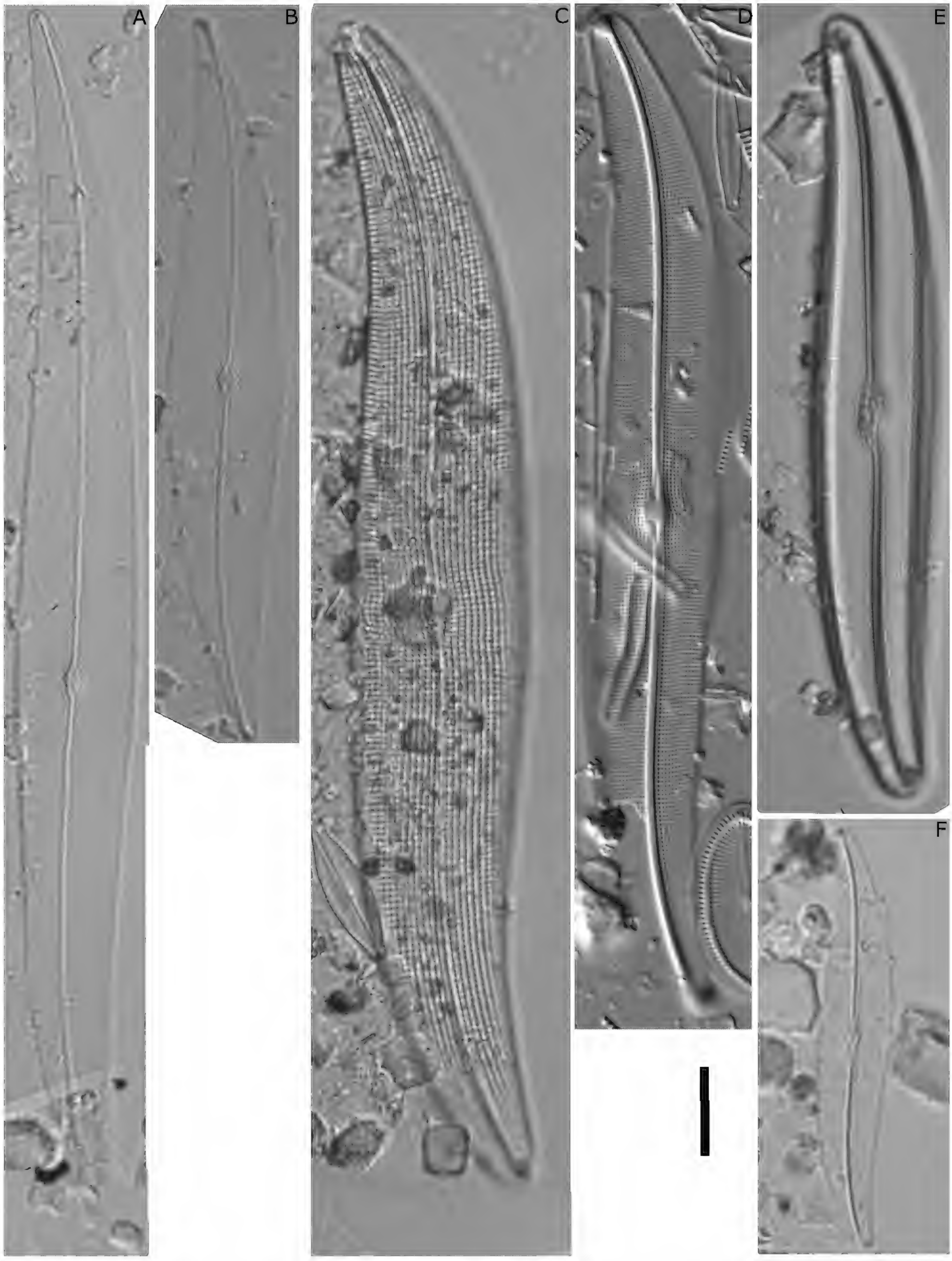

Figure 6. LM pictures of taxa found by morphological analyses. **A** *Pleurosigma* sp. 3. **B** *P.* sp. 1. **C** *Gyrosigma acuminatum.* **D** *G.* sp. 2. **E** *G.* cf. *sciotoense.* **F** *G.* sp. 1. Scale bar: 10 µm.

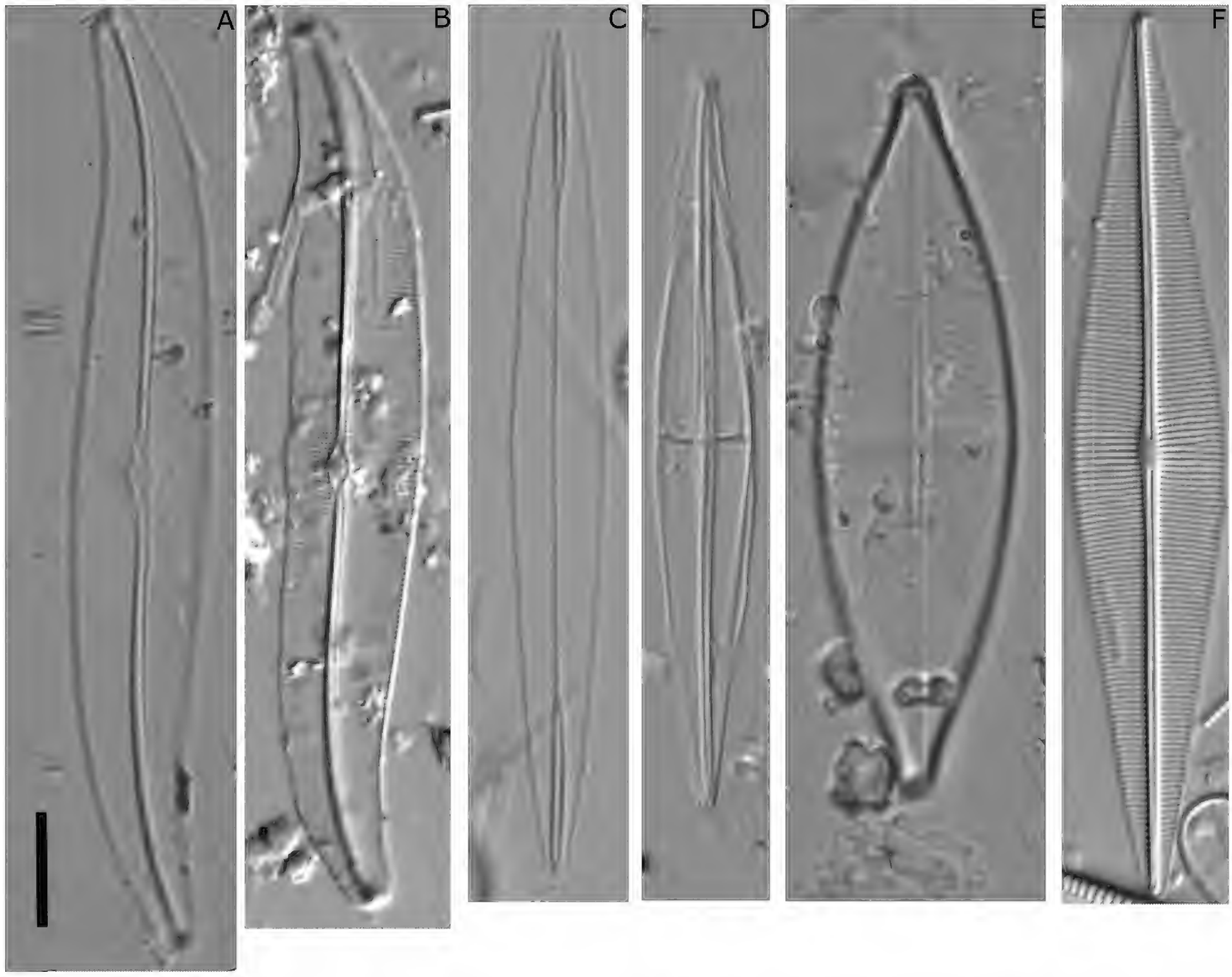

Figure 7. LM pictures of taxa found by morphological analyses. **A** *Gyrosigma* cf. *kuetzingii*. **B** *G*. cf. *scalproides*. **C** *Amphipleura pellucida*. **D** *Haslea spicula*. **E** *Parlibellus crucicula*. **F** *Craticula halophila*. Scale bar: 10 µm.

In total, 38 genera were retrieved in both datasets, with 21 genera identified only by morphological identification and 16 identified only by metabarcoding (Fig. 12).

The following genera were present only in the morphological analysis: *Amphipleura*, *Aulacoseira*, *Berkeleya*, *Caloneis*, *Craticula*, *Cyclostephanos*, *Envekadea*, *Fallacia*, *Hantzschia*, *Hippodonta*, *Luticola*, *Navicymbula*, *Parlibellus*, *Prestauroneis*, *Pseudofallacia*, *Scoliopleura*, *Sellaphora*, *Stauroneis*, *Synedropsis*, *Tabularia* and *Thalassiosira*.

While the genera found only in metabarcoding were: *Campylodiscus*, *Chaetoceros*, *Conticribra*, *Coscinodiscus*, *Cylindrotheca*, *Cymatopleura*, *Cymbopleura*, *Discostella*, *Eunotia*, *Fistulifera*, *Placoneis*, *Planothidium*, *Pseudostaurosira*, *Skeletonema*, *Staurosira* and *Tabellaria*.

Comparison of relative abundances

A comparison of the relative abundance of the most abundant taxa revealed differences between the two methods (Figs 14, 15). The taxa with the highest relative abundance of reads were: *Navicula directa*, *Cocconeis placentula* complex, NA (Fragilariophyceae), *Nitzschia palea*, and *Gomphonella olivacea* (≡ *Gomphonema olivaceum*). In terms of morphology, *Cocconeis placentula*

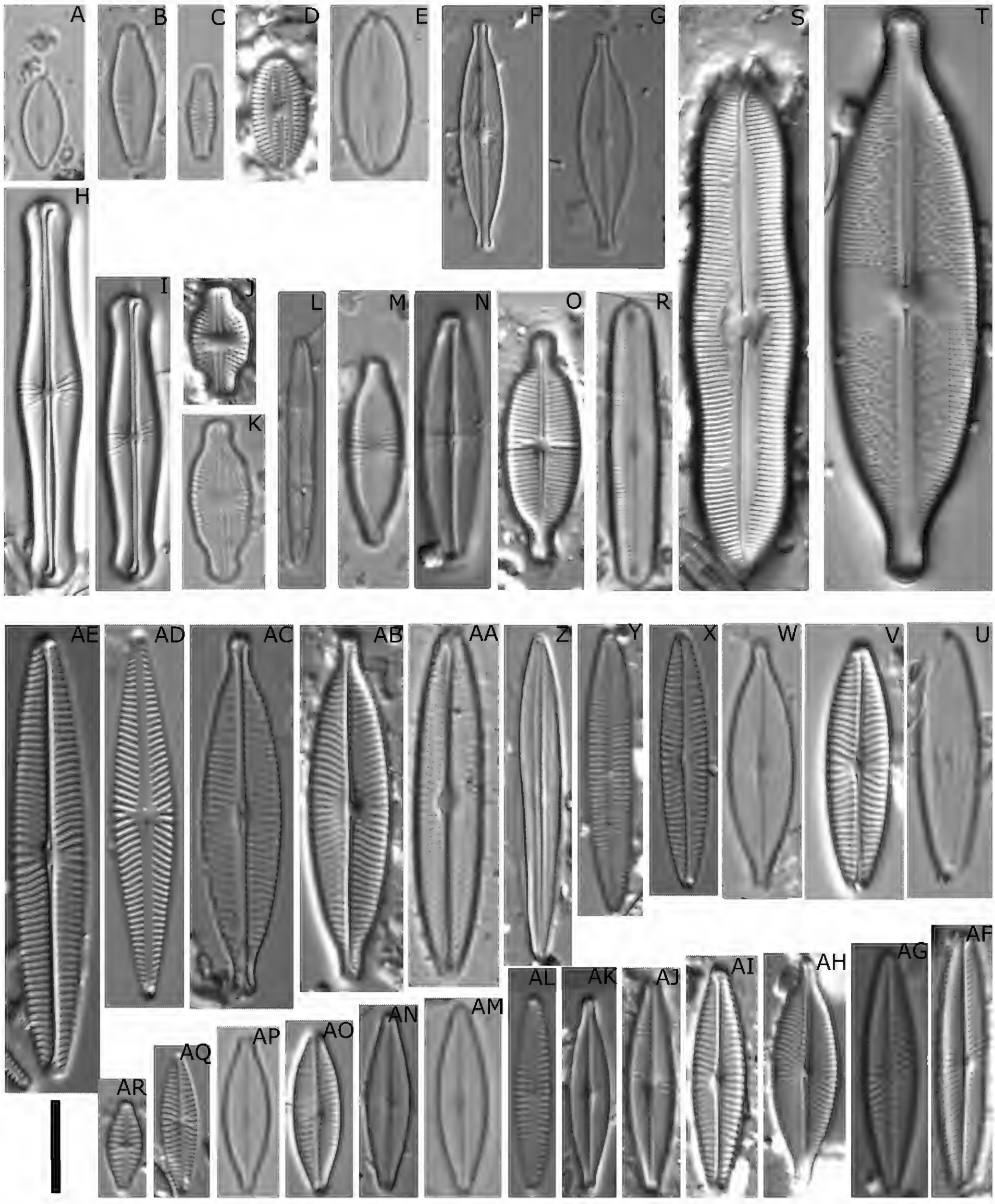

Figure 8. LM pictures of taxa found by morphological analyses. **A** *Craticula* cf. *subminuscula*. **B** *Hippodonta* sp. 1. **C** *Chamaepinnularia submuscicola*. **D** *Pseudofallacia* cf. *tenera*. **E** *Fallacia pygmaea* ssp. *Subpygmaea*. **F** *Brachysira neoexilis*. **G** *B.* cf. *neoexilis*. **H, I** *Envekadea hedinii*. **J** *Luticola ventriconfusa*. **K** *L. nivalis*. **L** *Berkeleya* sp. 1. **M** *Prestauroneis* sp. 1. **N** *P.* sp. 2 **O** *Prestauroneis furatensis*. **R** *Caloneis australis*. **S** *C. silicula*. **T** *Anomoeoneis sphaerophora*. **U** *Scoliopleura basrensis*. **V** *Navicula recens*. **W** *N. gregaria*. **X** *N. erifuga*. **Y** *N.* cf. *subagnita*. **Z** *N.* sp. 3. **AA** *N. escambia*. **AB** *N. rostellata*. **AC** *N. rhynchotella*. **AD** *N. wildii*. **AE** *N.* cf. *margalithii*. **AF** *N. simulata*. **AG** *N. cryptotenella*. **AH** *N. salinarum* var. *rostellata*. **AI** *N. cryptocephala*. **AJ** *N. vandamii* var. *vandamii*. **AK** *N.* sp. 4. **AL** *N.* spec. cf. *salinicola*. **AM** *N. veneta*. **AN** *N.* sp. 6. **AO** *N. phylleptosoma*. **AP** *N.* sp. 8. **AQ** *N.* cf. *cryptotenelloides*. **AR** *N. reichardtiana*. Scale bar: 10 µm.

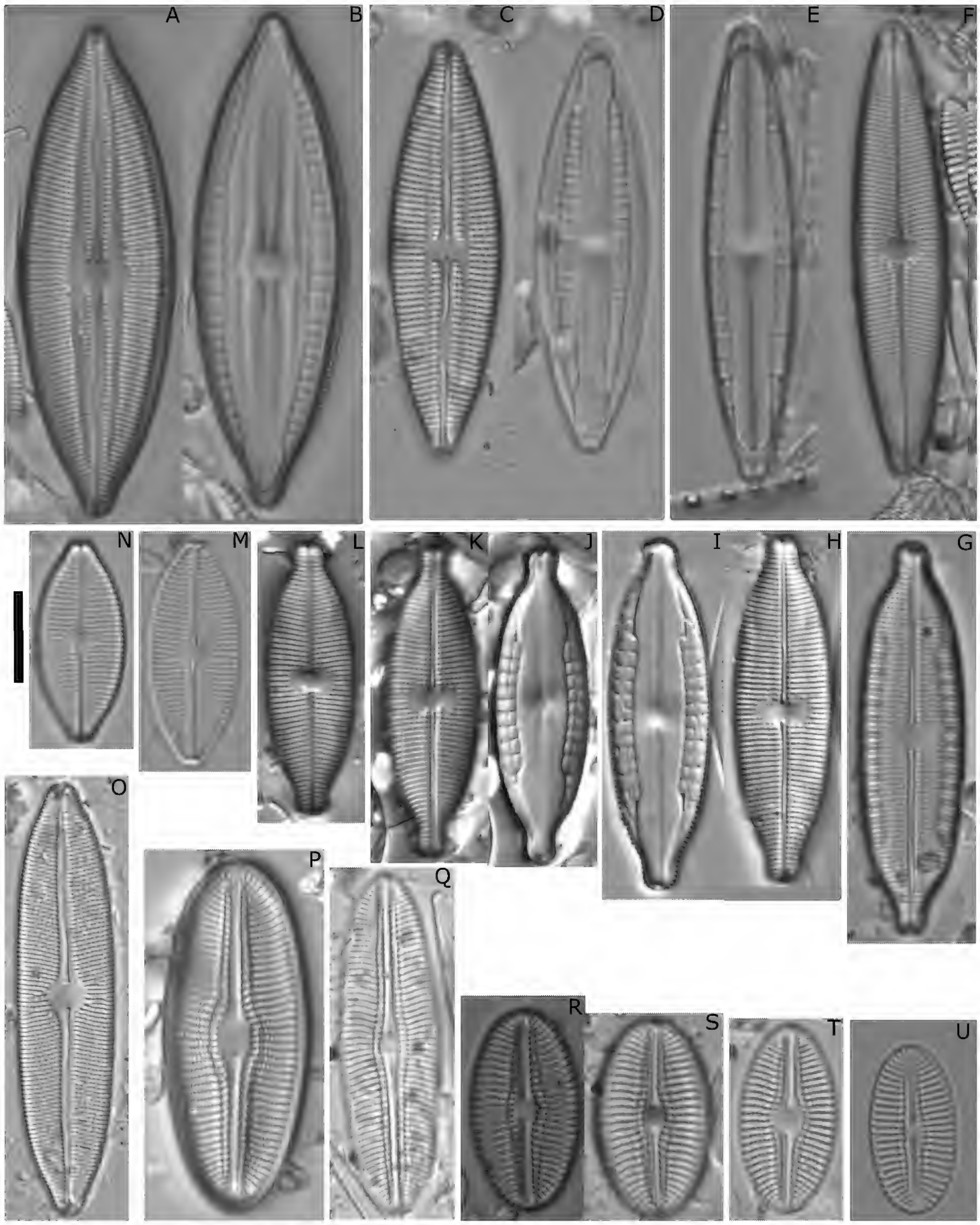

Figure 9. LM pictures of taxa found by morphological analyses. **A, B** *Mastogloia* cf. *brunii*. **C, D** *M. belaensis*. **E, F** *M. lacustris*. **G** *M.* aff. *smithii*. **H, I** *M.* cf. *smithii*. **J, K** *M. smithii*. **L** *M. sterijovskii*. **M** *M.* sp. 2. **N** *M.* sp. 1. **O** *M. elliptica*. **P** *Diploneis.* sp. 3. **Q** *D.* sp. 4. **R, S** *D.* sp. 1. **T** *D.* sp. 5. **U** *D.* sp. 2. Scale bar: 10 µm.

complex, *Achnanthidium minutissimum* complex, *Encyonopsis* cf. *microcephala*, *Tabularia fasciculata* and *Navicula recens* demonstrated the highest relative abundance of valves. The most common taxa of the microscopic analyses (relative abundances ≥ 1%), across Tigris samples were in decreasing order:

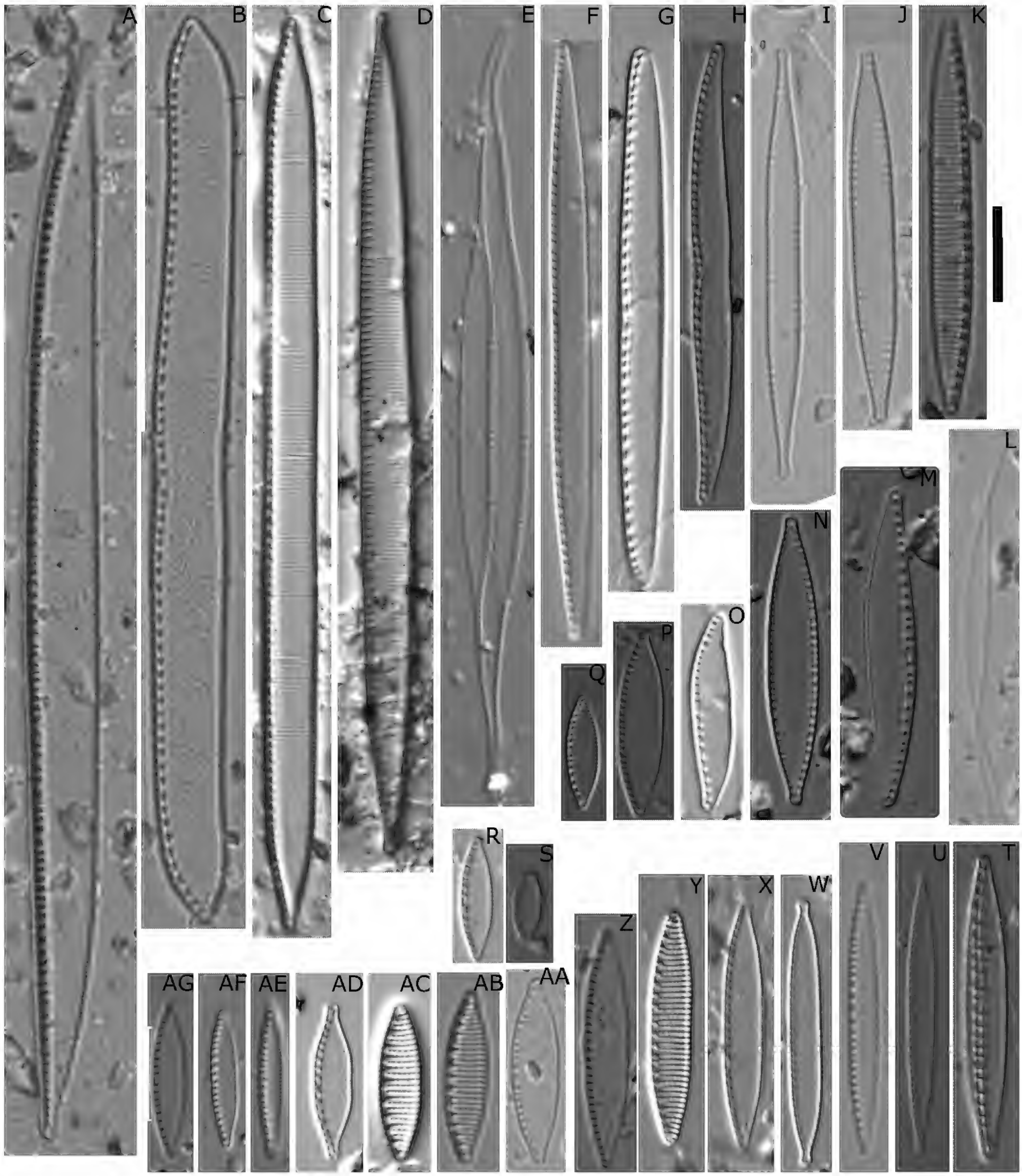

Figure 10. LM pictures of taxa found by morphological analyses. **A** *Nitzschia sigma*. **B** *N.* cf. *kurzeana*. **C** *N. intermedia*. **D** *N.* cf. *heufleriana*. **E** *N. reversa*. **F** *N. gracilis*. **G** *N. filiformis*. **H** *N. clausii*. **I** *N.* cf. *acicularioides*. **J** *N. palea*. **K** *N.* sp. 8. **L** *N.* sp.1. **M** *N. filiformis* var. *conferta*. **N** *N.* cf. *palea*. **O** *N.* cf. *clausi*. **P** *N.* cf. *solita*. **Q** *N. dealpina*. **R** *N.* sp. 6. **S** *N. inconspicua*. **T** *N. dissipata*. **U** *N. paleacea*. **V** *N. hantzschiana*. **W** *N. palea* var. *debillis*. **X** *N.* cf. *palea* var *debilis*. **Y** *N.* sp. 10. **Z** *N.* sp. 5. **AA** *N.* sp. 4. **AB** *N.* sp. 9. **AC** *N. amphibia*. **AD** *N. elegantula*. **AE** *N.* cf. *frustulum*. **AF** *N.* sp. 7. **AG** *N. bulnheimiana*. Scale bar: 10 µm.

Navicula recens (33.3%), *Cocconeis placentula* complex (23.9%) and *Navicula rostellata* (15.4%). Across Euphrates samples the most abundant taxa were: *Cocconeis placentula* complex (81%), *Achnanthidium minutissimum* complex (62.1%) and *Encyonopsis* cf. *microcephala* (60.7%).

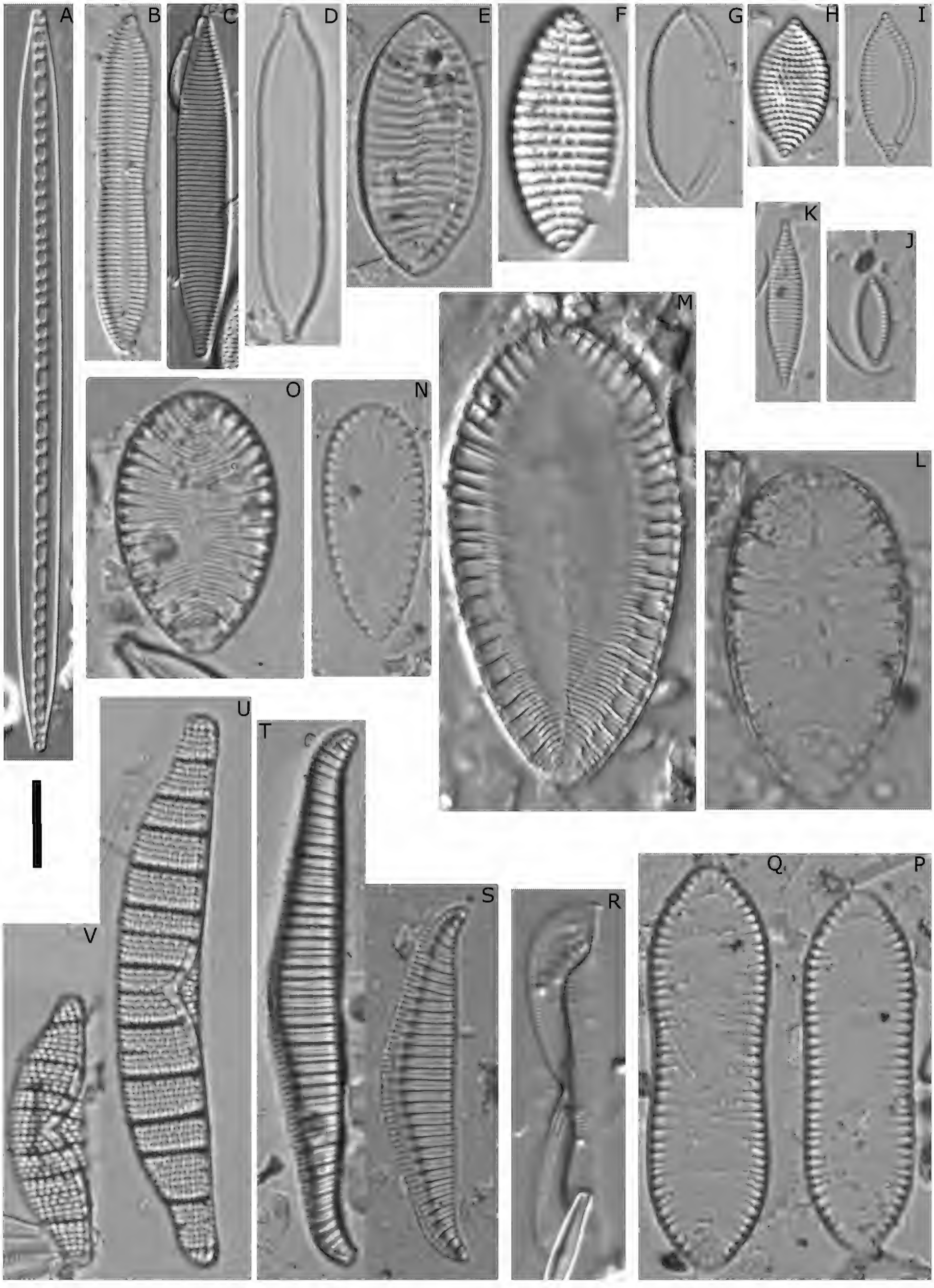

Figure 11. LM pictures of taxa found by morphological analyses. **A** *Bacillaria paxillifera*. **B** *Tryblionella hungarica*. **C** *T. angustata*. **D** *T. calida*. **E** *T. levidensis*. **F** *T. granulata*. **G** *T.* sp. 3. **H** *T. compressa*. **I** *T. compressa* var. *balatonis*. **J** *T.* sp. 1. **K** *T. angustatula*. **L** *Surirella striatula*. **M** *S. brightwellii*. **N** *S. neglecta*. **O** *S. brebissonii* var. *kuetzingii*. **P, Q** *S. librile*. **R** *Entomoneis* cf. *paludosa*. **S, T** *Rhopalodia gibba*. **U, V** *Epithemia adnata.* Scale bar: 10 µm.

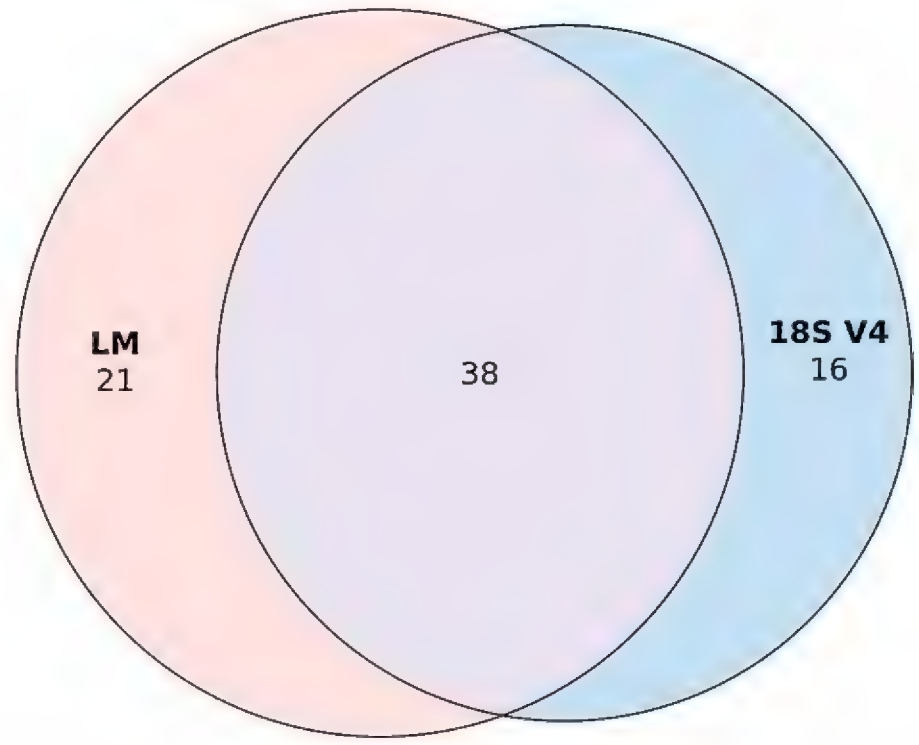

Figure 12. Venn diagrams comparing the performance of morphology and DNA metabarcoding in diatom identifications for genera.

Community analysis

According to the Shannon diversity index in the metabarcoding analysis (Table 1), the largest diatom diversity was found in winter in the River Euphrates at station E3 in sample 46, while the lowest values were recorded in summer in the River Euphrates E3 in sample 17. In the morphological analysis, the largest diatom diversity was found in summer in the River Euphrates at station E1 in sample 11, while the lowest values were recorded in winter in the River Euphrates E3 in sample 47. In general, the Shannon diversity indices were mostly higher in the metabarcoding analyses than in the morphological analyses.

Average taxa richness was also mostly higher in the metabarcoding than in the morphological analyses. In the metabarcoding analysis station W.E1.34 recorded the highest number of species (345), and station W.E3.43 the lowest number of species (5). In the morphological analysis, station S.E1.11 recorded the highest number of species (43), and station W.E3.47 the lowest number of species (11). Both approaches agreed that a low taxa richness was found in station E3 in Euphrates River and the highest richness in E1 in the same river.

For the samples collected from the Rivers Tigris and Euphrates the non–metric multidimensional scaling (NMDS) plots for morphology show a clear seasonal effect in community composition such as summer (= dry season) and winter (= rainy season) (Fig. 13, stress = 0.1). PERMANOVA confirmed a statistically significant differences in the community composition between the two seasons and the two rivers ($F = 2.61$, $p = 0.001$). This is in contrast to the NMDS plots for the 18SV4 analyses, where no clear seasonal effects in community composition for these samples were noted.

Discussion

Species composition by microscopy analysis

This study focused on epiphytic diatom taxa in the Euphrates-Tigris rivers, which are relatively shallow containing sediments covered by submerged macrophytes (Al-Handal et al. 2016), but no stones as habitats at the

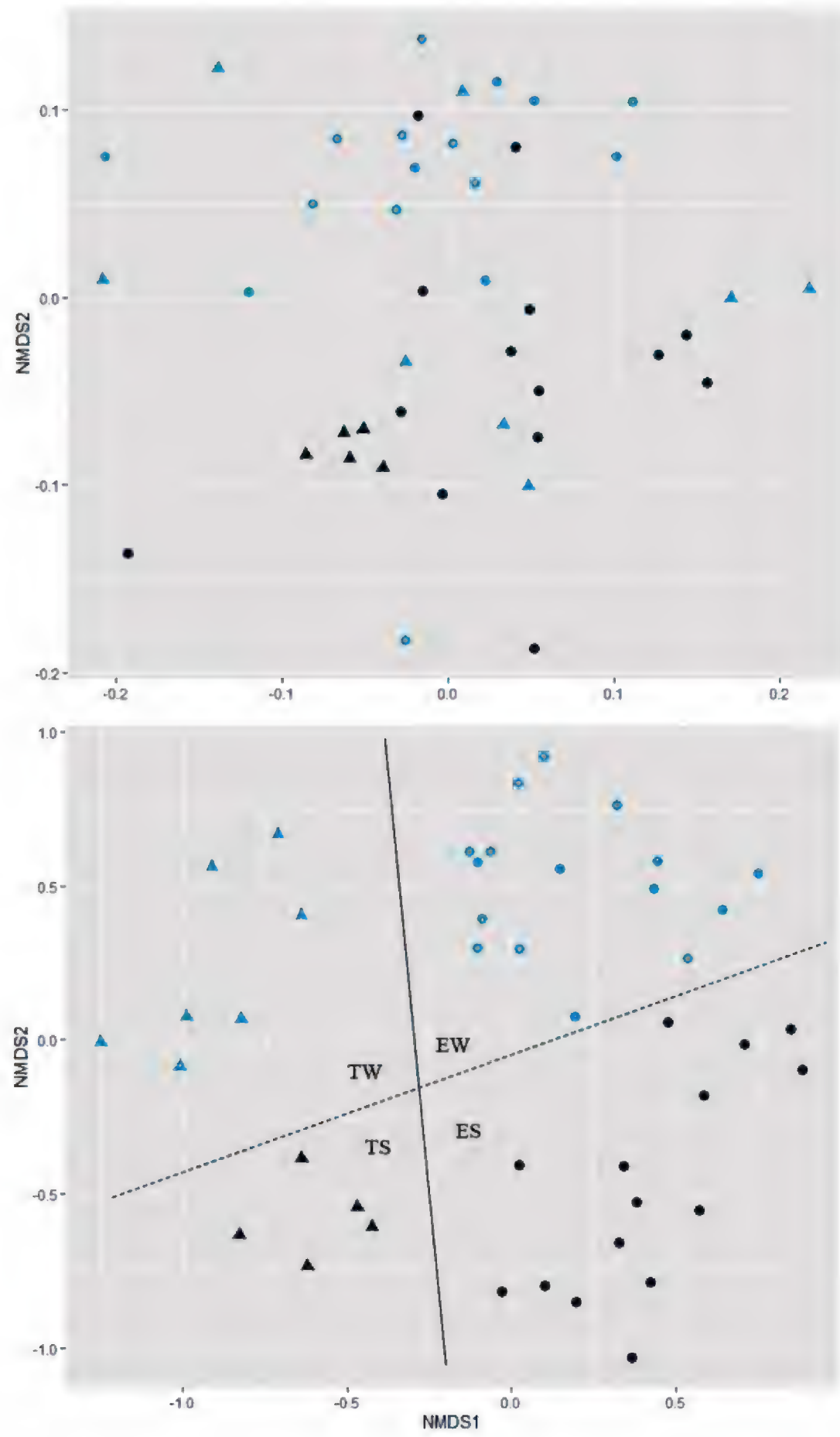

Figure 13. Non–metric Multidimensional Scaling (NMDS) multivariate clustering of epiphytic diatom communities based on the variables of season and sampling sites. Stress: 0.1. Observing a clear distinction line between the Rivers Tigris (T) and Euphrates (E), with the dashed line indicating the separation between summer (S) and winter (W). A 18 SV4 marker gene, B Morphology.

sampling stations. The results of the diatom analyses revealed a diverse epiphytic diatom community. With 284 taxa identified, the species richness observed in this study was notably higher than that reported in previous studies: Al-Shaheen and Al-Handal (2017) identified 193 taxa belonging to 70 genera; Al-Handal et al. (2014) found 74 species of epiphytic diatoms belonging to 38 genera, and Al-Handal and Abdullah (2010) recorded 116 taxa representing 49 genera. Such comparisons are challenging due to various factors, including the quantity of samples analyzed, in which season of the year they were taken, which substrates were studied and the taxonomic depth applied to the diatom analysis (Mora et al. 2017). The higher diversity observed in

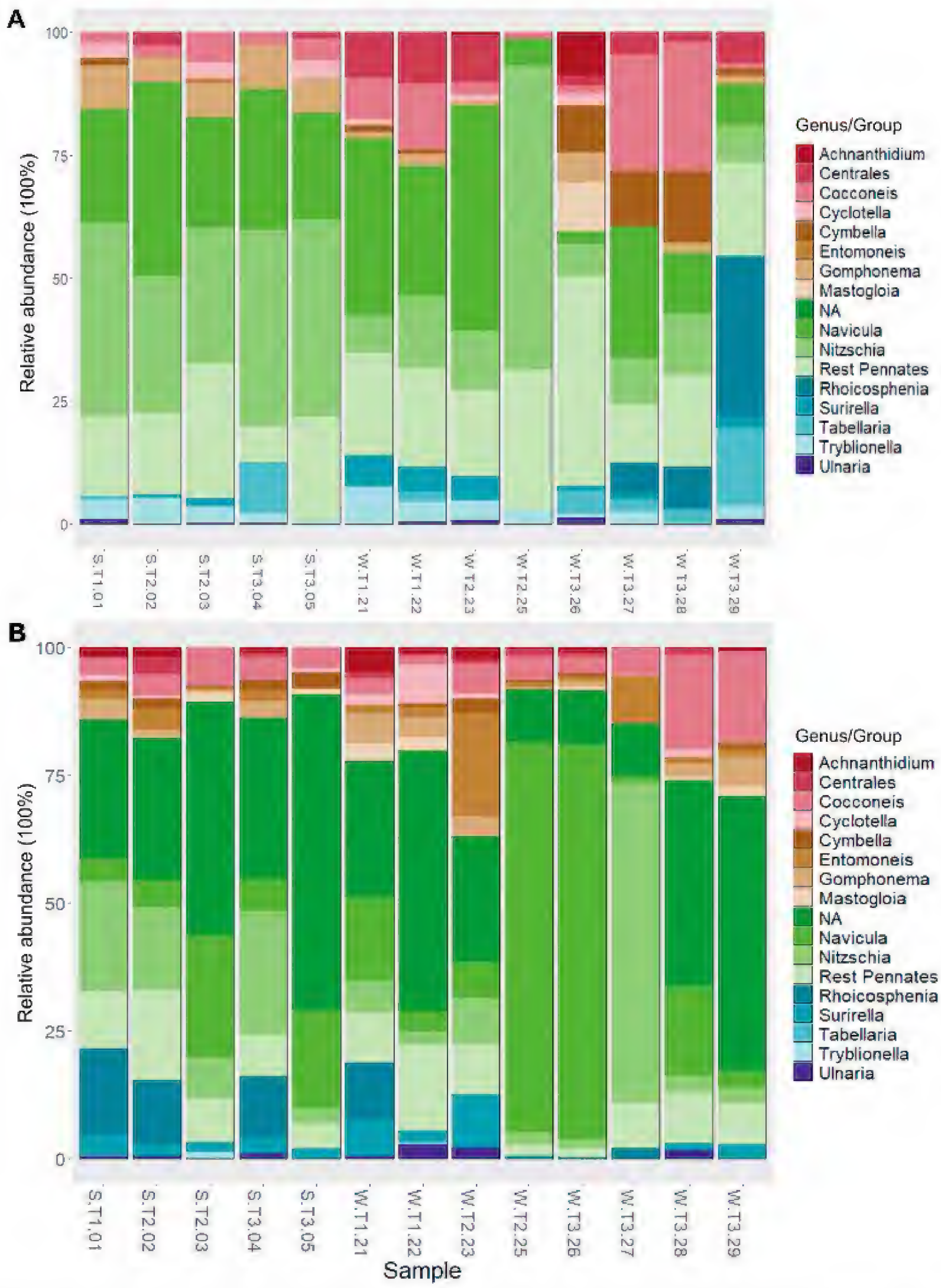

Figure 14. Relative abundance (%) of diatom genera across all sample locations for River Tigris. **A** Morphology. **B** 18SV4 marker gene. S: summer, W: winter.

our study can be attributed to the meticulous examination of samples using both microscopical instruments, LM and SEM, leading to the differentiation of several micromorphologically distinct taxa instead of grouping them into taxon complexes; although in some cases such as *Cocconeis placentula* and *Achnanthidium minutissimum* (for authors of species please consult Table 3) we had to use the term complex since currently data are missing for an internal differentiation.

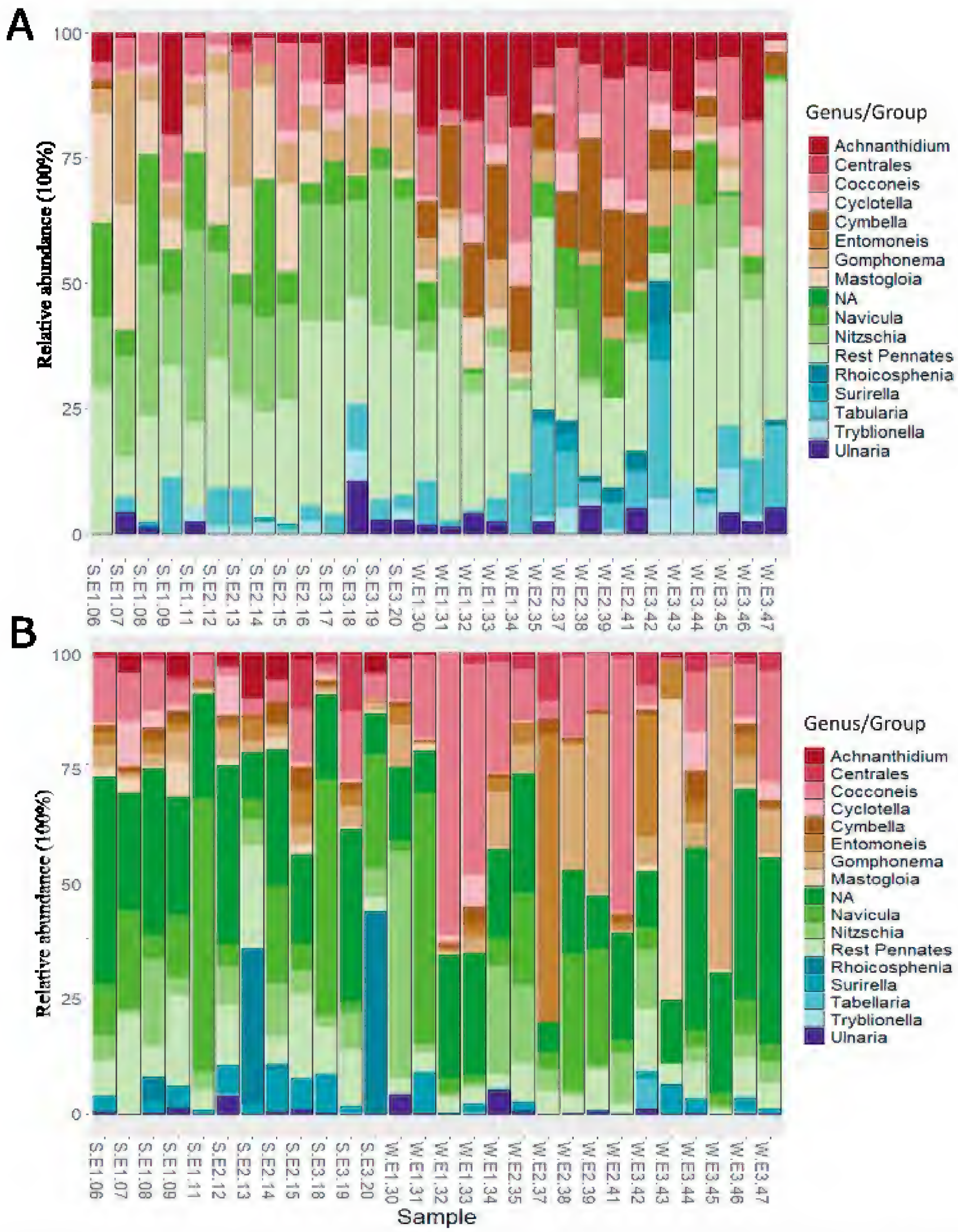

Figure 15. Relative abundance (%) of diatom genera across all sample locations for River Euphrates. **A** Morphology, **B** 18SV4 marker gene. S: summer, W: winter.

Altogether, 60% of the species were successfully identified. 18.5% of the taxa were categorized as ' cf. ' (confer). Additionally, 21.5% of the diatom community were designated as 'sp.' (species) pinpointing the need for further taxonomic investigation. This floristic list of this study includes 46 species recorded for the first time for the region (Table 3), underscoring the importance of this study in contributing to understanding the current diversity status of the local diatom flora. These discoveries can be attributed to ongoing alterations in

the rivers' environmental conditions, which prompt the disappearance or emergence of certain species such as the newly described *Prestauroneis furatensis* (Mohamad et al. in press) which was observed in summer samples of the River Euphrates. As expected for epiphytes, pennate diatoms dominated, constituting 93.7% of the identified species, while centric diatoms were only 6.3%. This is consistent with previous findings in freshwater environments (Al-Ahmady et al. 2019; Al-Saedy and Al-Shaheen 2021).

Several taxa of marine origin were recorded, including *Tabularia fasciculata*, *Seminavis strigosa*, *Navicula* cf. *subagnita*, *Tryblionella granulata*, *T. angustata*, *T. compressa*, *T. calida*, *Surirella striatula*, and *Entomoneis paludosa*. The reason may be the direct connection of the Qurna marsh with the Shatt Al-Arab River, coupled with its reception of water from the Arabian Gulf during high tides, creating a conduit for the migration of numerous marine diatoms to this region, situated around 200 km from the Gulf. This correlation is consistent with Al-Handal's 2010 study. Several brackish diatoms were found, such as *Bacillaria paxillifera*, *Tryblionella hungarica*, *Nitzschia filiformis*, *Navicula salinarum*, *Halamphora coffeaeformis* and *Haslea spicula*, because salinity fluctuates depending on the water flow rate. The years 2009 and 2014 showed an increase in temperatures leading to an enhanced evaporation and subsequently exacerbated the already pressing issue of salinity in the region (Al-Handal 2009; Al-Handal et al. 2014). With less freshwater flowing from the rivers, larger amounts of seawater ingress from the Arabian Gulf and add to the dilemma of salinity.

Nevertheless, in terms of ecological preferences, the distribution of diatom assemblages in the Rivers Tigris and Euphrates showcases a prevalence of freshwater (65.5%), followed by brackish (13.5%) and marine species (10%). This distribution is consistent with previous studies (Al-Handal et al. 2014; Al-Shaheen and Al-Handal 2017; Al-Saedy and Al-Shaheen 2021). The remaining 11% were euryvalent species, exhibiting a broad range of ecological preferences, spanning habitats from freshwater to marine environments, according to the literature (diatombase.org). The presence of taxa with varying, broad or uncertain ecological preferences further emphasizes the complex nature of these river ecosystems which encompass habitats ranging from freshwater to brackish and marine.

Species composition by metabarcoding analysis

Although metabarcoding has been extensively implemented worldwide in the past decade for diatom analysis, there is only one study (Al-Meshhdany and Hassan 2020) of this kind in the Tigris River in Iraq. Therefore, our study is the first of its kind to compare the traditional microscopic analysis and the molecular analysis (Metabarcoding) between the Rivers Tigris and Euphrates in Iraq. A fragment of 18S barcode gene (18SV4) combined with High-Throughput Sequencing, was employed to elucidate the composition for 47 samples and to compare these findings with traditional microscopic analyses.

This study showed that DNA metabarcoding is an efficient method and a reliable approach for evaluating diatom biodiversity, as it detected a nearly comparable number of genera to the traditional LM method. In contrast, DNA barcoding produced a higher number of ASVs compared to the taxa identified by LM.

This phenomenon can be attributed to several factors. Intraspecific genetic variation within diatom species can result in multiple ASVs being generated from slightly different sequences of the same species. Additionally, diatoms may possess multiple rRNA operons within their genomes, which can evolve at different rates and produce distinct sequences (Schloss 2021; Wang et al. 2024). Sequencing errors and PCR amplification artifacts also contribute to the generation of multiple ASVs from the same species (Kang et al. 2021). Furthermore, the incompleteness of reference databases, which may lack comprehensive or up-to-date sequences, can also lead to an overestimation of species diversity by not fully capturing the genetic variation within species. This highlights the need for more robust reference databases and careful interpretation of metabarcoding results (Schloss 2021).

Comparison between morphological and molecular results

The LM approach demonstrated greater efficiency in species-level identification. Consequently, the number of species-level identifications is lower in the metabarcoding dataset compared to the morphological analysis data. This finding aligns with Zimmermann et al. (2021), where 385 species were identified using the morphological approach, whereas 221 (*rbc*L) and 160 (18SV4) species were identified, respectively (e.g. Mora et al. 2019; Kulaš et al. 2022; Tapolczai et al. 2024). The differences in species-level identifications between the two methods can be primarily attributed to the gaps present in the reference databases, indicating their incompleteness, as well as the taxonomic inconsistencies within them. For example, in our study, most of the species in the genus *Mastogloia* and *Achnanthidium* given in the morphological results are not present in any reference library.

Interestingly, some taxa observed in metabarcoding were not detected in the morphological analyses, such as *Fistulifera*. These valves might have been destroyed during sample processing, as treatment with Naphrax tend to affect delicate structures (Vermeulen et al. 2012; Pérez-Burillo et al. 2022). Additionally, during the molecular analysis of our samples, *Navicula directa* was notably abundant, a species typically found in marine environments. Interestingly, this species was not observed in the morphological analysis of the same samples, where many marine species are increasingly found in freshwater ecosystems due to rising salinity levels (as mentioned above). The absence of *Navicula directa* in the morphological dataset raises concerns about the effectiveness of the 18SV4 marker used in this molecular analysis. This marker may have limitations in accurately differentiating between species, not only within the *Navicula* genus but also among some other diatom genera. The 18SV4 region is known to exhibit insufficient resolution for distinguishing closely related species due to high genetic similarity of this marker within certain closely related taxonomic groups. Such limitations could lead to overlooking of taxa, highlighting the need for supplementary markers to improve the resolution of molecular analyses.

Furthermore, some taxa with a high abundance and identified microscopically to the species level (e.g., *Navicula recens*, *Navicula rostellata* and *Nitzschia clausii*) which were to be expected in certain samples, had no corresponding match in the metabarcoding inventories. The reason may be the lack of appropriate concentrations of DNA in the corresponding sample.

Community analysis

Generally, the number of ASVs produced by DNA sequencing significantly differs from the taxa count identified morphologically in the same environmental samples (Pawlowski et al. 2014; Mora et al. 2019). This study revealed that the number of taxa per sample was often higher using metabarcoding compared to microscopy, a finding which aligns with several other studies (e.g., Tapolczai et al. 2024; Rimet et al. 2018). However, while some samples exhibited a higher taxonomic richness, this did not necessarily imply greater diversity. In some cases, metabarcoding identified fewer species compared to microscopy.

Various biological, environmental, and technical factors contribute to the overestimation or underestimation of taxonomic richness in metabarcoding data. The natural infraspecific and intragenomic variability of the barcode marker is considered one of the most significant biological factors influencing overestimation of richness. This poses a particular challenge when a single recognized species or taxonomic indicator encompasses a diverse array of genetic patterns. Sequences corresponding to different genetic patterns within the same taxon may cluster into different ASVs, artificially inflating taxonomic richness (Mora et al. 2019).

NMDS plots of 18SV4 inventories did not show a seasonal effect in the community composition for samples collected from the Rivers Tigris and Euphrates. In contrast, the NMDS plots for morphology revealed a clear seasonal effect distinguishing between summer (dry seasons) and winter (rainy seasons). This discrepancy may be attributed to gaps in the reference databases of DNA barcode sequences, particularly at the species level, which hinder accurate taxonomic assignments.

To address these limitations, it might be valuable to repeat the study using the *rbc*L marker, which has shown promise in providing higher resolution for diatom identification (e.g., Schimani et al. 2023). The *rbc*L marker may help to resolve the discrepancies observed with the 18SV4 marker and offer a clearer understanding of seasonal variations in diatom communities. Additionally, producing unialgal diatom strains from the studied sites and incorporating their data into the study could provide further insights into the diversity and dynamics of diatom populations, as unialgal strains allow for more detailed morphological and genetic analyses (Mohamad et al. 2022). The gaps in reference libraries need to be closed by cultured diatoms of the region to improve the accuracy of species identification, thereby enhancing the overall reliability of the metabarcoding approach in assessing diatom community composition.

Conclusion

In this study, we investigated the epiphytic diatom assemblages in the Euphrates and Tigris catchment area using the method metabarcoding in comparison with microscopical morphology (LM and SEM). Both methods revealed a high diversity of diatoms, however, significant differences were found in the taxon lists. Our results demonstrate that a combination of metabarcoding and microscopy, increases the detection and identification of diatom species, highlighting the importance of using both approaches complementary. Even in the advent of big advances and successes in the development and standardization of molecular tools for biodiversity assessments and monitoring (Apothéloz-Perret-Gentil et al.

2017), the role of morphology in species discovery and detection remains central. Further studies using additional markers, such as *rbc*L, are recommended to enhance our understanding of diatom diversity. Additionally, diatoms strains isolated from the studied area could provide deeper insights into their ecological roles and responses to environmental changes. Such investigations are essential for illustrating the importance of sustainable ecosystem management and the conservation of the vital resource of water, both regionally and globally. By highlighting the complex biodiversity of diatoms and their sensitivity to environmental shifts, this study underscores the need for effective conservation strategies to maintain the health and sustainability of aquatic ecosystems.

Additional information

Conflict of interest

The authors have declared that no competing interests exist.

Ethical statement

No ethical statement was reported.

Funding

Heba Mohamad gratefully acknowledges funding by a scholarship by the Heinrich Böll Stiftung [P139825]. We acknowledge support by the Open Access Publication Fund of Freie Universität Berlin.

Author contributions

HM, RJ, JZ developed the concept of this study. MAS sampled and measured the parameters. HM did the identifications with NA and AAH supporting. HM, KS and JZ performed the metabarcoding analysis. HM did the corresponding graphics, figures and tables. NA and WHK are responsible for the curation and data curation. HM wrote the manuscript. The manuscript was commented, edited, and finally accepted by all authors.

Author ORCIDs

Heba Mohamad https://orcid.org/0000-0002-3217-3067
Katherina Schimani https://orcid.org/0000-0003-2125-0239
Maitham Al-Shaheen https://orcid.org/0000-0003-1535-5333
Nélida Abarca https://orcid.org/0000-0001-8897-160X
Regine Jahn https://orcid.org/0000-0002-3833-3746
Adil Al-Handal https://orcid.org/0000-0003-4703-7823
Wolf-Henning Kusber https://orcid.org/0000-0003-4543-5764
Jonas Zimmermann https://orcid.org/0000-0002-0522-0569

Data availability

All of the data that support the findings of this study are available in the main text.

References

Al-Ahmady S, Al-Abbawy D, Al-Shaheen M (2019) Relationships between environmental variables and both of planktonic and epiphytic diatoms in the East Hammar marshes, Southern Iraq. Marsh Bulletin 14(1): 22–43.

Al-Handal AY (2009) Littoral diatoms from the Shatt Al-Arab estuary, North West Arabian Gulf. Cryptogamie. Algologie 30(2): 153–183.

Al-Handal AY, Abdullah D (2010) Diatoms from the restored Mesopotamian marshes, South Iraq. Algological Studies 133: 65–103. https://doi.org/10.1127/1864-1318/2010/0133-0065

Al-Handal AY, Al-Shaheen MA (2019) Diatoms in the wetlands of Southern Iraq. Bibliotheca Diatomologica 67: 1–252.

Al-Handal AY, Abdullah D, Wulff A, Abdulwahab MT (2014) Epiphytic diatoms of the Mesopotamian wetland: Huwaiza marsh, South Iraq. Diatom 30: 1–15.

Al-Handal AY, Taffs K, Abdullah D, Zawadzki A (2016) Vertical distribution of diatoms in the sediment of Al-Huwaiza Marsh, Southern Iraq and their use as indicators of environmental changes. Algological Studies 150(1): 53–76. https://doi.org/10.1127/algol_stud/2016/0239

Al-Handal AY, Al-Shaheen MA, Al-Saedy R, Wulff A (2022) *Synedropsis abuflosensis* sp. nov., a new araphid diatom (Bacillariophyceae) from the Shatt Al-Arab River, Southern Iraq. Cryptogamie, Algologie 43(2): 31-39. https://doi.org/10.5252/cryptogamie-algologie2022v43a2

Al-Meshhdany WY, Hassan FM (2020) Five diatom species identified by using potential application of next generation dna sequencing. Bulletin of the Iraq Natural History Museum 16(1): 39–61. https://doi.org/10.26842/binhm.7.2020.16.1.0039

Al-Saedy R, Al-Shaheen MA (2021) Tolerance of benthic diatoms to severe environmental stress: A case study in Shatt Al-Arab River, Basrah, Iraq. Biological and Applied Environmental Research 5(2): 222–247. https://doi.org/10.51304/baer.2021.5.2.222

Al-Shaheen MA (2016) Taxonomical and Ecological Study on the Diatoms Communities of Shatt Al-Arab River, Southern Iraq. PhD Thesis, College of Science, University of Basrah, Iraq.

Al-Shaheen MA, Al-Handal AY (2017) Influence of Environmental Variables and Different Hosting Substrates on Diatom Assemblages in the Shatt Al-Arab River, Southern Iraq. Biological and Applied Environmental Research V(1): 69-87.

Almandoz GO, Fabro E, Sprong P, Mascioni M, Antoni J, Ferrario M, Metfies K, Barrera FM (2024) Metabarcoding and microscopy characterization of phytoplankton from frontal areas of the Argentine Sea. Frontiers in Marine Science V: 10. https://doi.org/10.3389/fmars.2023.1306336

APHA American Public Health Association (1999) Standard methods for examination of water and wastewater. 20th edn, Washington, DC, USA.

APHA American Public Health Association (2005) Standard methods for examination of water and wastewater. 21st edn, Washington, DC, USA.

Apothéloz-Perret-Gentil L, Cordonier A, Straub F, Iseli J, Esling P, Pawlowski J (2017) Tax onomy-free molecular diatom index for high-throughput eDNA biomonitoring. Molecular Ecology Resources 17(6): 1231–1242. https://doi.org/10.1111/1755-0998.12668

Bailet B, Bouchez A, Franc A, Frigerio J-M, Keck F, Karjalainen S-M, Rimet F, Schneider S, Kahlert M (2019) Molecular versus morphological data for benthic diatoms biomon itoring in Northern Europe freshwater and consequences for ecological status. Metabarcoding and Metagenomics 3: e34002. https://doi.org/10.3897/mbmg.3.34002

Battarbee R, Carvalho L, Jones V, Flower R, Cameron N, Bennion H, Juggins S (2001) Tracking Environmental Change Using Lake Sediments: Terrestrial, Algal and Siliceous Indicators. Kluwer Academic Publishers.

Bíró T, Duleba M, Földi A, Kiss KT, Orgoványi P, Trábert Z, Vadkerti E, Wetzel CE, Ács É (2022) Metabarcoding as an effective complement of microscopic studies in revealing the composition of the diatom community – a case study of an oxbow lake of Tisza River (Hungary) with the description of a new *Mayamaea* species. Metabarcoding and Metagenomics 6: 319–336. https://doi.org/10.3897/mbmg.6.87497

Burki F, Sandin MM, Jamy M (2021) Diversity and ecology of protists revealed by metabarcoding. Current Biology 31(19): R1267–R1280. https://doi.org/10.1016/j.cub.2021.07.066

Callahan BJ, McMurdie PJ, Rosen MJ, Han AW, Johnson AJA, Holmes SP (2016) DADA2: High resolution sample inference from illumina amplicon data. Nature Methods 13(7): 581–583. https://doi.org/10.1038/nmeth.3869

Gemeinholzer B, Droege G, Zetzsche H, Haszprunar G, Klenk H-P, Güntsch A, Berendsohn W, Wägele JW (2011) The DNA Bank Network: The start from a German initiative. Biopreservation and Biobanking 9(1): 51–55. https://doi.org/10.1089/bio.2010.0029

Guiry MD, Guiry GM (2024) AlgaeBase. World-wide electronic publication, University of Galway. https://www.algaebase.org [searched on 21. March 2024]

Hadi SIIA, Santana H, Brunale PPM, Gomes TG, Oliveira MD, Matthiensen A, Brasil BSAF (2016) DNA barcoding green microalgae isolated from neotropical in land waters. PLoS ONE 11(2): e0149284. https://doi.org/10.1371/journal.pone.0149284

Hashim BM, Al Maliki A, Abd Alraheem E, Al-Janabi AMS, Halder B, Yaseen ZM (2022) Temperature and precipitation trend analysis of the Iraq Region under SRES scenarios during the twenty-first century. Theoretical and Applied Climatology 148(3-4): 881–898. https://doi.org/10.1007/s00704-022-03976-y

Hassan FM, Maysoon MS, Awaz BM (2010) A limnological study in Euphrates River from Al-Hindiya barrage to Al- Kifil city, Iraq. Basrah Journal of Sciences 28(2): 273–288.

Jahn R, Kusber WH, Skibbe O, Zimmermann J, Van AT, Buczkó K, Abarca N (2019) *Gomphonella olivacea* (Bacillariophyceae) – a new phylogenetic position for a well-known taxon, its typification, new species and combinations. Plant Ecology and Evolution 152(2): 219–247. https://doi.org/10.5091/plecevo.2019.1603

Kang W, Anslan S, Börner N, Schwarz A, Schmidt R, Künzel S, Rioual P, Echeverría-Galindo P, Vences M, Wang J, Schwalb A (2021) Diatom metabarcoding and microscopic analyses from sediment samples at Lake Nam Co, Tibet: The effect of sample-size and bioinformatics on the identified communities. Ecological Indicators 121: 107070. https://doi.org/10.1016/j.ecolind.2020.107070

Keck F, Vasselon V, Rimet F, Bouchez A, Kahlert M (2018) Boosting DNA metabarcoding for biomonitoring with phylogenetic estimation of operational taxonomic units' ecological profiles. Molecular Ecology Resources 18(6): 1299–1309. https://doi.org/10.1111/1755-0998.12919

Kelly M, Juggins S, Mann DG, Sato S, Glover R, Boonham N, Sapp M, Lewis E, Hany U, Kille P, Jones T, Walsh K (2020) Development of a novel metric for evaluating di atom assemblages in rivers using DNA metabarcoding. Ecological Indicators 118: e106725. https://doi.org/10.1016/j.ecolind.2020.106725

Krammer K, Lange-Bertalot H (1986) Bacillariophyceae, Teil 1. Naviculaceae. In: Ettl H, Gerloff J, Heyning H, Mollenhauer D (Eds) Süsswasserflora von Mitteleuropa 2/1. Gustav Fischer Verlag, Heidelberg, 1–876.

Krammer K, Lange-Bertalot H (1988) Bacillariophyceae: Bacillariaceae, Epithemiaceae, Surirellaceae. In: Ettl H, Gerloff J, Heyning H, Mollenhauer D (Eds) Süsswasserflora von Mitteleuropa Vol. 2/2. Gustav Fischer Verlag, Jena.

Krammer K, Lange-Bertalot H (1991) Bacillariophyceae: Centrales, Fragilariaceae, Eunotiaceae. In: In: Ettl H, Gerloff J, Heyning H, Mollenhauer D (Eds) Süßwasserflora von Mitteleuropa Vol. 2/3. Gustav Fischer Verlag, Stuttgart.

Krammer K (2002) *Cymbella*. In: Lange-Bertalot H (Ed.) Diatoms of Europe 3. A.R.G. Gantner Verlag K.G., Ruggell, 1–584.

Kulaš A, Udovič MG, Tapolczai K, Žutinić P, Orlić S, Levkov Z (2022) Diatom eDNA metabarcoding and morphological methods for bioassessment of karstic river. The Science of the Total Environment 829: e154536. https://doi.org/10.1016/j.scitotenv.2022.154536

Lange-Bertalot H (2001) Diatoms of Europe. Diatoms of the European Inland Waters and Comparable Habitats. Vol 2: *Navicula* sensu stricto. 10 genera separated from *Navicula* sensu lato. Frustulia. Diatoms of Europe 2: 526. [A.R.G. Ganter-Verlag K.G., Königstein, Deutschland]

Lange-Bertalot H, Hofmann G, Werum M, Cantonati M, Kelly M (2017) Freshwater benthic diatoms of Central Europe: over 800 common species used in ecological assessment. Koeltz Botanical Books Schmitten-Oberreifenberg, 942 pp.

Larsson J (2021) eulerr: Area-Proportional Euler and Venn Diagrams with Ellipses. R package version 6.1.1. https://CRAN.R-project.org/package=eulerr

Lee S, Gaiser E, Van de Vijver B, Edlund MB, Spaulding SA (2014) Morphology and typification of *Mastogloia smithii* and *M. lacustris*, with descriptions of two new species from the Florida Everglades and the Caribbean region. Diatom Research 31(2): 325–350. https://doi.org/10.1080/0269249X.2014.889038

Levkov Z (2009) *Amphora* sensu lato. In: Lange-Bertalot H (Ed.) Diatoms of Europe Vol. 5. A.R.G. Gantner Verlag K.G., Ruggell, 916 pp.

Levkov Z, Metzeltin D, Pavlov A (2013) Diatoms of the European inland waters and comparable habitats. *Luticola* and *Luticolopsis*. Diatoms of Europe 7. Koeltz Scientific Books, Königstein, 1–698.

Levkov Z, Mitić-Kopanja D, Reichardt E (2016) Diatoms of the European inland waters and comparable habitats. The diatom genus *Gomphonema* in the Republic of Macedonia. Diatoms of Europe 8. Koeltz Botanical Books, Oberreifenberg, 1–552.

Lind GT (1979) Handbook of common methods in limnology 2nd edn., London, 1991 pp.

Liu J, Rühland KM, Chen J, Xu Y, Chen S, Chen Q, Huang W, Xu Q, Chen F, Smol JP (2017) Aerosol-weakened summer monsoons decrease lake fertilization on the Chinese Loess Plateau. Nature Climate Change 7(3): 190–194. https://doi.org/10.1038/nclimate3220

Malviya S, Scalco E, Audic S, Vincent F, Veluchamy A, Poulain J, Wincker P, Iudicone D, de Vargas C, Bittner L, Zingone A, Bowler C (2016) Insights into global diatom distribution and diversity in the world's ocean. Proceedings of the National Academy of Sciences of the United States of America 113(11): E1516. https://doi.org/10.1073/pnas.1509523113

Martin M (2011) Cutadapt removes adapter sequences from high-throughput sequencing reads. EMBnet.Journal 17(1): 10–12. https://doi.org/10.14806/ej.17.1.200

Maulood BK, Hassan FM, Al-Lami AA, Toma JJ, Ismail AM (2013) Checklist of algal flora in Iraq. Ministry of Environment, Baghdad, 100 pp.

McMurdie PJ, Holmes S (2013) phyloseq: An R package for reproducible interactive analysis and graphics of microbiome census data. PLoS ONE 8(4): e61217. https://doi.org/10.1371/journal.pone.0061217

Metzeltin D, Lange-Bertalot H, García-Rodríguez F (2005) Diatoms of Uruguay. Compared with other taxa from South America and elsewhere. In: H. Lange-Bertalot (Ed.) Iconographia Diatomologica. Annotated Diatom Micrographs. Vol. 15. Taxonomy-Biogeography-Diversity. A.R.G. Gantner Verlag K.G. 15, 736 pp.

Mohamad H, Mora D, Skibbe O, Abarca N, Deutschmeyer V, Enke N, Kusber W-H, Zimmermann J, Jahn R (2022) Morphological variability and genetic marker stability of 16 monoclonal pennate diatom strains under medium-term culture. Diatom Research 37(4): 307–328. https://doi.org/10.1080/0269249X.2022.2141346

Mohamad H, Jahn R, Al-Handal A, Al-Shaheen M, Kusber WH, Zimmermann J, Abarca N (in press) *Prestauroneis furatensis* sp. nov., a new diatom species from the River Euphrates, Iraq. Fottea.

Mora D, Carmona J, Jahn R, Zimmermann J, Abarca N (2017) Epilithic diatom communities of selected streams from the Lerma-Chapala Basin, Central Mexico, with the description of two new species. PhytoKeys 88: 39-69. https://doi.org/10.3897/phytokeys.88.14612.

Mora D, Abarca N, Proft S, Grau JH, Enke N, Carmona J, Skibbe O, Jahn R, Zimmermann J (2019) Morphology and metabarcoding: A test with stream diatoms from Mexico highlights the complementarity of identification methods. Freshwater Science 38(3): 448–464. https://doi.org/10.1086/704827

Mortágua A, Vasselon V, Oliveira R, Elias C, Chardon C, Bouchez A, Rimet F, João Feio M, Almeida SFP (2019) Applicability of DNA metabarcoding approach in the bioassessment of Portuguese rivers using diatoms. Ecological Indicators 106: e105470. https://doi.org/10.1016/j.ecolind.2019.105470

Nistal-García A, García-Garcíab P, García-Giróna J, Borrego-Ramosc M, Blancoa S, Bécaresa E (2021) DNA metabarcoding and morphological methods show complementary patterns in the metacommunity organization of lentic epiphytic diatoms Alejandro. The Science of the Total Environment 786: 147410. https://doi.org/10.1016/j.scitotenv.2021.147410

Oksanen J, Blanchet FG, Friendly M, Kindt R, Legendre P, McGlinn D, Minchin P, O'Hara R, Simpson G, Solymos P (2022) vegan: Community Ecology Package. R package version 2.5-7. 2020.

Pavlov A, Jovanovska E, Wetzel CE, Ector L, Levkov Z (2016) Freshwater *Mastogloia* (Bacillariophyceae) taxa from Macedonia, with a description of the epizoic M. sterijovskii sp. nov. Diatom Research 31(2): 85–112. https://doi.org/10.1080/0269249X.2016.1157376

Pawlowski J, Esling P, Lejzerowicz F, Cedhagen T, Wilding TA (2014) Environmental monitoring through protist next-generation sequencing metabarcoding: Assessing the impact of fish farming on benthic foraminifera communities. Molecular Ecology Resources 14(6): 1129–1140. https://doi.org/10.1111/1755-0998.12261

Pérez-Burillo J, Trobajo R, Vasselon V, Rimet F, Bouchez A, Mann DG (2020) Evaluation and sensitivity analysis of diatom DNA metabarcoding for WFD bioassessment of Mediterranean rivers. The Science of the Total Environment 727: e138445. https://doi.org/10.1016/j.scitotenv.2020.138445

Pérez-Burillo J, Valoti G, Witkowski A, Prado P, Mann DG, Trobajo R (2022) Assessment of marine benthic diatom communities: insights from a combined morphological–metabarcoding approach in Mediterranean shallow coastal waters. Marine Pollution Bulletin 174: 113183. https://doi.org/10.1016/j.marpolbul.2021.113183

Pinseel E, Kulichová J, Scharfen V, Urbánková P, Van de Vijver B, Vyverman W (2019) Extensive cryptic diversity in the terrestrial diatom *Pinnularia borealis* (Bacillariophyceae). Protist 170(2): 121–140. https://doi.org/10.1016/j.protis.2018.10.001

Piredda R, Claverie JM, Decelle J, de Vargas C, Dunthorn M, Edvardsen B, Eikrem W, Forster D, Kooistra WHCF, Logares R, Massana R, Montresor M, Not F, Ogata H, Pawlowski J, Romac S, Sarno D, Stoeck T, Zingone A (2018) Diatom diversity through

HTS–metabarcoding in coastal European seas. Scientific Reports 8(1): e18059. https://doi.org/10.1038/s41598-018-36345-9

Reichardt E (2001) Revision der Arten um *Gomphonema truncatum* und *G. capitatum*. In: Jahn R, Kociolek JP, Witkowski A, Compère P (Eds) Lange-Bertalot-Festschrift, Studies on Diatoms. A.R.G. Gantnter Verlag K.G. Ruggell, 187–224.

Reichardt E (2018) Die Diatomeen im Gebiet der Stadt Treuchtlingen. Bayerische Botanische Gesellschaft 1: 1–576.

Rimet F, Abarca N, Bouchez A, Kusber W-H, Jahn R, Kahlert M, Keck F, Kelly MG, Mann DG, Piuz A, Trobajo R, Tapolczai K, Vasselon V, Zimmermann J (2018) The potential of high throughput sequencing (HTS) of natural samples as a source of primary taxonomic information for reference libraries of diatom barcodes. Fottea 18(1): 37–54. https://doi.org/10.5507/fot.2017.013

Rimet F, Gusev E, Kahlert M, Kelly MG, Kulikovskiy M, Maltsev Y, Mann DG, Pfannkuchen M, Trobajo R, Vasselon V, Zimmermann J, Bouchez A (2019) Diat.barcode, an open-access curated barcode library for diatoms. Scientific Reports 9(1): 1–12. https://doi.org/10.1038/s41598-019-51500-6

Rivera SF, Vasselon V, Ballorain K, Carpentier A, Wetzel CE, Ector L, Bouchez A, Rimet F (2018) DNA metabarcoding and microscopic analysis of sea turtles biofilms: Complementary to understand turtle behavior. PLoS ONE 13(4): e0195770. https://doi.org/10.1371/journal.pone.0195770

Round FE, Crawford RM, Mann DG (1990) The diatoms, biology and morphology of the genera. Cambridge University Press, UK, 747 pp.

Rovira L, Trobajo R, Sato S, Ibáñez C, Mann DG (2015) Genetic and physiological diversity in the diatom *Nitzschia inconspicua*. The Journal of Eukaryotic Microbiology 62(6): 815–832. https://doi.org/10.1111/jeu.12240

Ruppert KM, Kline RJ, Rahman Md S (2019) Past, present, and future perspectives of environmental DNA (eDNA) metabarcoding: A systematic review in methods, monitoring, and applications of global eDNA. Global Ecology and Conservation 17: e00547. https://doi.org/10.1016/j.gecco.2019.e00547

Schimani K, Abarca N, Kusber WH, Skibbe O, Campana GL, Mohamad H, Jahn R, Zimmermann J (2023) Exploring benthic diatom diversity in the West Antarctic Peninsula: Insights from a morphological and molecular approach. Metabarcoding and Metagenomics 7: 339–384. https://doi.org/10.3897/mbmg.7.110194

Schloss PD (2021) Amplicon Sequence Variants Artificially Split Bacterial Genomes into Separate Clusters. MSphere 6(4): e00191–e21. https://doi.org/10.1128/mSphere.00191-21

Smucker NJ, Edlund MB, Vis ML (2008) The distribution, morphology, and ecology of a non-native species, *Thalassiosira lacustris* (Bacillariophyceae), from benthic stream habitats in North America. Nova Hedwigia 87(1–2): 201–220. https://doi.org/10.1127/0029-5035/2008/0087-0201

Strickland JDH, Parsons TR (1972) A practical handbook of seawater analysis, 2nd edn. Bulletin Fishery Research Board of Canada, 167 pp.

Stuart J, Ryan KG, Pearman JK, Thomson-Laing J, Hampton HG, Smith KF (2024) A comparison of two gene regions for assessing community composition of eukaryotic marine microalgae from coastal ecosystems. Scientific Reports 14(1): 6442. https://doi.org/10.1038/s41598-024-56993-4

Tapolczai K, Chonova T, Fidlerov´ D, Makovinsk´ J, Mora D, Weigand A, Zimmermann J (2024) Molecular metrics to monitor ecological status of large rivers: Implementa-

tion of diatom DNA metabarcoding in the Joint Danube Survey 4. Ecological Indicators V(160): 111883. https://doi.org/10.1016/j.ecolind.2024.111883

Trobajo R, Mann DG, Clavero E, Evans KM, Vanormelingen P, McGregor RC (2010) The use of partial cox1, rbcL and LSU rDNA sequences for phylogenetics and species identification within the *Nitzschia palea* species complex (Bacillariophyceae). European Journal of Phycology 45(4): 413–425. https://doi.org/10.1080/09670262.2010.498586

Van de Vijver B, Fofana Ch, Sow EH, Cocquyt C, Blanco S, Ector L (2017) Morphology of two *Mastogloia* species (Bacillariophyta) from Lac de Guiers (Senegal) and comparison with the type material of *M. braunii*. European Journal of Taxonomy 374(374): 1–23. https://doi.org/10.5852/ejt.2017.374

Vasselon V, Rimet F, Tapolczai K, Bouchez A (2017) Assessing ecological status with dia toms DNA metabarcoding: Scaling–up on a WFD monitoring network (Mayotte island, France). Ecological Indicators 82: 1–12. https://doi.org/10.1016/j.ecolind.2017.06.024

Vermeulen S, Lepoint G, Gobert S (2012) Processing samples of benthic marine dia toms from Mediterranean oligotrophic areas. Journal of Applied Phycology 24(5): 1253–1260. https://doi.org/10.1007/s10811-011-9770-4

Visco JA, Apothéloz-Perret-Gentil L, Cordonier A, Esling P, Pillet L, Pawlowski J (2015) Environmental Monitoring: Inferring the Diatom Index from Next-Generation Sequencing Data. Environmental Science & Technology 49(13): 7597–7605. https://doi.org/10.1021/es506158m

Wang H, Liu K, He Z, Chen Y, Hu Z, Chen W, Leaw CP, Chen N (2024) Extensive intragenomic variations of the 18S rDNA V4 region in the toxigenic diatom species Pseudo-*nitzschia* multistriata revealed through high-throughput sequencing. Marine Pollution Bulletin 201: 116198. https://doi.org/10.1016/j.marpolbul.2024.116198

Witkowski A, Lange-Bertalot H, Metzeltin D (2000) Diatom Flora of Marine Coasts I. Iconographia Diatomologica 7. Koeltz Scientific Books, 925 pp.

Zidarova R, Kopalová K, Van de Vijver B (2016) Ten new Bacillariophyta species from James Ross Island and the South Shetland Islands (Maritime Antarctic Region). Phytotaxa 272(1): 37. https://doi.org/10.11646/phytotaxa.272.1.2

Zimmermann J, Jahn R, Gemeinholzer B (2011) Barcoding diatoms: Evaluation of the V4 subregion on the 18S rRNA gene, including new primers and protocols. Organisms, Diversity & Evolution 11(3): 173–192. https://doi.org/10.1007/s13127-011-0050-6

Zimmermann J, Glöckner G, Jahn R, Enke N, Gemeinholzer B (2015) Metabarcoding vs. morphological identification to assess diatom diversity in environmental studies. Molecular Ecology Resources 15(3): 526–542. https://doi.org/10.1111/1755-0998.12336

Zimmermann J, Mora D, Tapolczai K, Proft S, Chonova T, Rimet F, Bouchez A, Fidlerová D, Makovinská J, Weigand A (2021) Metabarcoding of phytobenthos samples. Scientific Report: A Shared Analysis of the Danube River. JDS4, 145–156.

Zinger L, Lionnet C, Benoiston A-S, Donald J, Mercier C, Boyer F (2021) metabaR: An r package for the evaluation and improvement of DNA metabarcoding data quality. Methods in Ecology and Evolution 12(4): 586–592. https://doi.org/10.1111/2041-210X.13552